UNIVERSITY OF CALIFORNIA, SAN DIEGO

Modulation of proton-coupled electron-transfer reactions in azurin: quantum yield and pK_a analyses

A thesis submitted in partial satisfaction of the requirements for the degree

Master of Science

in

Chemistry

by

Bethany Corrine Larson

Committee in charge:

Professor Judy Kim, Chair
Professor Michael Tauber
Professor Ulrich Müller

2013

The Thesis of Bethany Corrine Larson is approved, and it is acceptable in quality and form for publication on microfilm and electronically:

Chair

University of California, San Diego

2013

DEDICATION

To my family and my two best friends, for pushing me to persevere both directly and indirectly and going beyond themselves to help me be who I am today.

TABLE OF CONTENTS

Signature Page iii

Dedication iv

Table of Contents v

List of Figures ix

List of Tables xi

Acknowledgements xii

Abstract of the Thesis xv

1 Introduction 1

1.1 Electron transfer theory in biomolecules 1

1.2 Amino acid radical intermediates 5

1.3 Proton-coupled electron transfer theory 5

1.4 Azurin as model protein for biological electron transfer 8

1.5 Nitrotyrosine as an unnatural amino acid in biomolecules 10

2 Materials and Methods 13

2.1 Preparation of azurin protein 13

2.1.1 Primer design and site-directed mutagenesis 13

2.1.2 Transformation of PCR product 13

2.1.3 Isolation of plasmid DNA 14

2.1.4 Preparation of cell stocks 14

2.1.5 Azurin protein expression 17

2.1.6 Lysis of cells to isolate azurin protein 17

2.1.7 FPLC Purification of copper azurin 18

2.1.8 Potassium cyanide dialysis of azurin 22
2.1.9 Nitration of azurin 24
2.2 Azurin sample preparation for spectroscopic experiments 26
2.2.1 Preparation of model NAYA and azurin samples for spectrophotometric titration 26
2.2.2 Preparation of azurin samples for photolysis 26
2.3 Experimental instrumentation and calculations 27
2.3.1 Photolysis instrumentation and set-up 27
2.3.2 Calculating tyrosine pK_as 28
2.3.3 Calculation of tyrosine and nitrotyrosine ε_{280} 29
2.3.4 Calculations of W48• quantum yield 29
2.3.5 Potassium ferrioxalate actinometry 33
3 pK_as of native tyrosines 34
3.1 Introduction 34
3.2 Materials and methods 35
3.2.1 Preparation of model NAYA and azurin samples for spectrophotometric titration 35
3.2.2 Calculating tyrosine pK_as 35
3.3 Results 36
3.3.1 Titration of tyrosine residues; structural basis for anomalously high pK_a values 36
3.3.2 MD simulation studies of single-tyrosine mutants 40
3.3.3 Titration of nitrated copper single-tyrosine mutants 43

3.4 Discussion....46

4 Photolysis of zinc azurin in the presence of exogenous quenchers....50

4.1 Introduction....50

4.2 Materials and methods....51

4.2.1 Preparation of azurin samples for photolysis....51

4.2.2 Calculation of W48• quantum yields....51

4.2.3 Potassium ferrioxalate actinometry....52

4.3 Results....52

4.3.1 Photolysis of ZnW48 and CuAz....52

4.3.2 Photolysis of ZnW48 and CuW48 with $Ru^{III}(NH_3)_6Cl_2$ exogenous quencher....57

4.3.3 Photolysis of ZnW48 and CuW48 with $[Co^{III}(NH_3)_5Cl]^{2+}$ exogenous quencher....60

4.3.4 Photolysis of ZnW48 and CuW48 with N_2O....65

4.3.5 pH dependent photolysis of ZnW48 with $[Co^{III}(NH_3)_5Cl]^{2+}$....68

4.4 Discussion....69

5 W48• quenching studies....77

5.1 Introduction....77

5.2 Materials and methods....78

5.2.1 Preparation of single-tyrosine mutants and nitrotyrosine mutants....78

5.2.2 Preparation of samples for photolysis and photolysis set-up....78

5.2.3 Calculation of W48• quantum yields 79
5.3 Results 79
5.3.1 Photolysis of single-tyrosine mutants 79
5.3.2 Photolysis of ZnF110Y 81
5.3.3 Photolysis of nitrotyrosine 81
5.4 Discussion 83
6 Conclusion and Future studies 89
6.1 Summary 89
6.2 Future studies 93
Resources 95

LIST OF FIGURES

Figure 1.1: Electron tunneling timetable 4

Figure 1.2: Thermodynamic scheme for oxidation and deprotonation of tyrosine and tryptophan 7

Figure 1.3: Crystal structure of wild-type azurin 9

Figure 1.4: Absorption spectra of nitrotyrosine and nitrotyrosinate 12

Figure 2.1: Potassium cyanide dialysis of $Cu^{II}Az$ 23

Figure 2.2: Samples of successfully nitrated CuY72 and unsuccessfully nitrated CuY72 with tetranitromethane byproduct 25

Figure 3.1: Crystal structure of wild-type azurin with relative distance from Y72 and Y108 to W48 38

Figure 3.2: Absorption spectra of tyrosine titration and pK_a curves for CuWT and single-tyrosine mutants 39

Figure 3.3: Wild-type azurin crystal structure illustrating local environment surrounding Y108 42

Figure 3.4: Molecular dynamic simulations illustrating local environments of Y72 and Y108 42

Figure 3.5: Absorption spectra of nitrotyrosine titration 44

Figure 3.6: Spectrophotometric titration curves for $Y72NO_2$ and $Y108NO_2$ 45

Figure 4.1: Absorption spectra of photolyzed ZnW48 and CuW48 56

Figure 4.2: Absorption spectra of photolyzed 1:2, CuW48/ZnW48 mixture 56

Figure 4.3: Absorption spectra of photolyzed $Cu^{I}W48/[Ru^{III}(NH_3)_6]^{2+}$ mixture ... 59

Figure 4.4: Difference absorption spectra of $CuW48/[Co^{III}(NH_3)_5Cl]^{2+}$ mixture .. 61

Figure 4.5: Absorption spectra of $[Co^{III}(NH_3)_5Cl]^{2+}$, $[Co^{II}(NH_3)_5Cl]^{2+}$ and NATA 63

Figure 4.6: Change in absorbance of W48• with time from ZnW48/$[Co^{III}(NH_3)_5Cl]^{2+}$mixture 64

Figure 4.7: Absorbance spectra of ZnW48/$[Co^{III}(NH_3)_5Cl]^{2+}$mixture 64

Figure 4.8: Difference absorption spectra of ZnW48/ $Co^{III}(NH_3)_5Cl]^{2+}$mixture with and without N_2O gas 67

Figure 4.9: Absorption spectra of ZnW48/ $Co^{III}(NH_3)_5Cl]^{2+}$mixture before and after scaled subtraction of closed-shell W48 74

Figure 5.1: Absorption spectra of ZnY72 and ZnY72NO_2 before and after photolysis 82

Figure 5.2: Pathways for charge transfer from Y72 and Y108 to W48 85

Figure 5.3: Model for electron transfer and deprotonation pathways of tryptophan and tyrosine in azurin 86

LIST OF TABLES

Table 2.1: Thermal cycler method for PCR.....15

Table 2.2: Recipes for microbiology media 16

Table 2.3: Equilibration method for FPLC system.....19

Table 2.4: Summary of azurin samples.....21

Table 2.5: List of relevant extinction coefficients.....32

Table 4.1: Summary of W48• quantum yields with various exogenous quenchers.....54

Table 5.1: Summary of W48• quantum yields for azurin mutants.....80

ACKNOWLEDGEMENTS

I would firstly like to acknowledge my advisor, Professor Judy Kim, for being an admirable example of a teacher and scientist and for ultimately believing in my abilities as a researcher. I joined Judy's lab with little exposure to an academic research setting, and will always be appreciative that she allowed me to be a part of the group with the intent of expanding my knowledge and experiences as a chemist. The dynamics of the lab facilitated a comfortable learning environment for all members, and much of this can be credited to Judy's patience and enthusiasm for science as well as her direct involvement in our experimental set-ups. I will always be grateful for her confidence in me and for providing me with the opportunities to take ownership of my project and pursue my Master's degree.

I also need to thank Professor Michael Tauber for being a scientist who shows meticulous dedication to addressing issues that are often overlooked. Several of my experiments were made possible via use of his lab's resources, and his expertise in spectroscopy helped bring us to important conclusions on the azurin research project. In addition, I admire his patience and am grateful for the value that he, as well as Judy, place on teaching and on a student's education. I can only hope that future members of both Judy and Mike's labs are appreciative of the instrumental guidance that they have to offer.

Dr. Brian Leigh has also been an important part of my graduate student career through his mentorship on all aspects of sciences. Our lab has been able to comfortably ask Brian questions related to almost any scientific theory or experimental procedure, allowing us to effectively learn from his experiences so that we are able to become more

successful scientists. His knowledge and familiarity with the science surrounding azurin promoted helpful conversations and guided several parts of my project. In addition to all of his valuable help and encouraging words, Brian also brought an abundance of necessary laughter to the group.

As an undergraduate, I began my research in the lab working with Dr. Hannah Shafaat, an intelligent and highly motivated scientist. She taught me all of the necessary basics on azurin and helped me establish hypotheses that I pursued further as a graduate student. I also was given the opportunity to work closely with Jennifer Pomponio, a very hard-working scientist who became a great research partner as we helped each other analyze foundational questions for the improvement of each of our research projects. I will always be appreciative of her as well as Greg Shimamura, Rachel Kim, and Kent Truong's hard work towards the overall azurin research project.

I'd also like to thank several members of the Kim group, including Dr. Diana Schlamadinger, Guipeun Kang, Ignacio López-Peña, Weihan Cao, and Saajan Bhakta for their helpful advice and encouraging words. In addition, I want to thank the Tauber group for contributing to the fun and uplifting dynamics of the lab environment.

Other members of the department who I would like to thank are Annette Medina from Prof. Akif Tezcan's group for her help in operating the ICP-OES at SIO as well as Pat Blachly from Prof. Andy McCammon's group for his helpful discussions and for providing MD simulations.

Lastly, I'd like to thank my parents who have always been my biggest support and motivation to pursue my personal goals. I am very thankful for their trust in me and their acceptance of my mistakes, and am appreciative of their continued love and

encouragement. Chris has been the best teammate I could ask for, and I am so blessed to have been able to pursue science alongside him – he is by far one of the most patient individuals I know and I am so grateful that he's always believed in me.

ABSTRACT OF THE THESIS

Modulation of proton-coupled electron-transfer reactions in azurin: quantum yield and pK_a analyses

by

Bethany Corrine Larson

Master of Science in Chemistry

University of California, San Diego, 2013

Professor Judy Kim, Chair

Long-range electron transfer (ET) reactions are central to many biochemical processes. To accomplish these long-range reactions, biomolecules often utilize multi-step ET processes via redox-active intermediates such as tryptophan and tyrosine. Azurin

is a type I blue copper protein with two tyrosines (Y108 and Y72) and one tryptophan (W48), and serves as a model to study ET in proteins. Upon UV-photoexcitation of a tyrosine deficient and zinc (II)-substituted azurin mutant (ZnW48) in the presence of an exogenous electron quencher, W48 ejects an electron and forms a stable neutral radical, W48•. The quantum yield for formation of W48• depends on the identity of the exogenous quencher, namely Cu^{II}Azurin, $Ru^{III}(NH_3)_6Cl_2$, or $[Co^{III}(NH_3)_5Cl]^{2+}$. In WTAzurin, the presence of the two tyrosines reduced the yield of W48• formation. This observation motivated further studies of ET reactions involving tyrosine, more specifically proton-coupled electron transfer (PCET) in which there is simultaneous transfer of the electron and phenolic proton in order to avoid high-energy intermediates. To understand potential PCET pathways, spectrophotometric titrations were performed on Y72 and Y108, both of which were found to have anomalously high pK_a values. In an attempt to observe decoupled proton and electron transfer events at physiological pH values, the unnatural amino acid, nitrotyrosine, was incorporated into azurin, decreasing pK_as by ~ 5 pH units. Photolysis of a sample of $ZnNO_2Y72$ with an exogenous quencher further decreased the yield of W48•. These studies shed light on the importance of amino acid radical intermediates in facilitating long-range electron transfer in more complex biological systems.

1 Introduction

1.1 Electron transfer theory in biomolecules

Biological electron transfer (ET) is an essential component to life. In most cases, these events take place between and within proteins, and rely on the dynamic and static protein structures to dictate thermodynamic parameters. Amino acids, the building blocks of protein biomolecules, not only determine the final folded structure of proteins, but also control vital electron transfer pathways by their inherent molecular properties, such as charge and hydrophobicity. Nature has uniquely modified protein structure by careful selection of amino acid sequences in order to optimize electron transfer pathways and rates, resulting in effective biological reactions. By utilizing amino acid intermediates, electron transfer reactions can occur at tremendous rates within the microsecond time regime that would otherwise take seconds or longer; such long timescales would prohibit effective biological reactions from taking place.[1]

Semi-classical theory surrounding electron transfer has been studied for several decades. Rudolf Marcus won the Nobel Prize in 1992 for his work involving the theory of electron transfer reactions, and since then the theory of electron transfer in proteins has become a highly studied area of research.[3, 4] The key idea behind electron transfer as proposed by Marcus is based on the Arrhenius equation for rates of chemical reactions. In the equation for electron transfer rates (Equation 1.1), the formula maintains dependence on the Gibbs free energy (ΔG^o), Boltzmann constant (k_b), and temperature (T) but also includes new parameters including the reorganization energy, λ (energy required for the

reactants to have the same nuclear configuration as the products), and H_{AB} (the electronic coupling between the D and A).

$$k_{ET} = \sqrt{\frac{4\pi^3}{h^2 \lambda k_B}} H_{AB}^2 \exp\left\{-\frac{(\Delta G^0 + \lambda)^2}{4\lambda k_B T}\right\} \quad (1.1)$$

In this equation, it becomes evident that the relationship between ΔG^o and λ controls the barrier of ET, and the ET rate is at a maximum when ΔG^o is equal to λ. This equation also shows that the rate of reaction not only depends on driving force but also the change in nuclear geometry due to the fact that the rate begins to decrease as the driving force exceeds the reorganization energy. This predicted reversal in behavior was termed the "inverted region" by Marcus.

The mechanisms of electron transfer in proteins has been investigated and simplified most recently by Beratan, Onuchic, and Hopfield.[5] In their research, they discussed the electron tunneling pathway (TP) in proteins where the donor and acceptor interaction is mediated primarily by covalent (through bond) interactions as well as through-space interactions.[5, 6] Covalent interactions are dictated by amino acid polarity and hydrophobicity and contribute significantly to the electronic coupling between donor and acceptor. Unlike the uniform barrier (UB) model which averages the bridge distance between D and A while disregarding the composition,[7] the TP model suggests the importance of amino acid sequence on the rate of electron transfer, where in conjunction with theoretical framework, experimental research can assess ET rates more clearly through site-directed mutagenesis.[6-8]

Electron transfer in proteins also largely depends on the distance between donor and acceptor. In an electron transfer pathway, the overall rate depends on the rate of each

charge-transfer step, which has an exponential dependence on distance.[9] Because electron transport can occur over great distances (>25 Å), multi-step electron tunneling via charged intermediates is necessary in order to sustain efficient redox activity in biomolecules at rates that are orders of magnitude faster than if there were no intermediates.[10] Long-range electron transport is therefore made possible provided that these intermediates maintain high enough potentials to exhibit satisfactory rates for redox activity. When ET is achieved via this multi-step, or hopping, mechanism, movement of an electron across 20 Å can occur via two short 10 Å steps, each of which takes place on the picosecond timescale, as opposed to the single-step tunneling rate of microseconds.[1] (see Fig. 1.1).

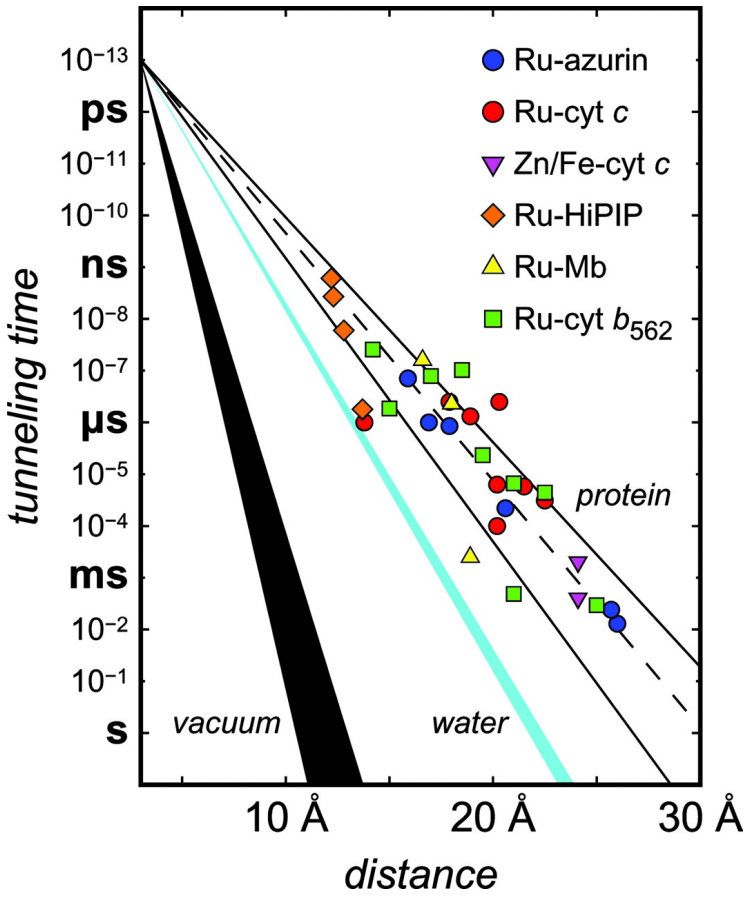

Figure 1.1: Tunneling timetable for select proteins in various media. The proteins are ruthenium-modified (azurin, cytochrome c, HiPIP, myoglobin, and cytochrome b562) and a mixture of Zn and Fe cytochrome c. Image abstracted from Gray, H.B., Winkler, J.R. Long-range electron transfer. PNAS. 2005.

1.2 Amino acid radical intermediates

Accomplishing fast electron transfer rates in biological redox enzymes is a well-studied area of research. Nature has evolved to incorporate charged intermediates, or more specifically amino acid radical intermediates, to overcome the barrier of charge separation over long distances. The most common amino acids that play integral roles in long-range electron transfer are tryptophan and tyrosine, both of which exist as radical intermediates. In fact, these radicals are of vital importance in proteins such as photosystem II and ribonucleotide reductase. The first tyrosyl radical discovered, TyrZ, is located in photosystem II and plays a vital role in oxygen evolution by first reducing $P680^{+}$, creating a hole that is then filled by oxidation of water in the Mn complex on a ns – μs time scale.[11] Ribonucleotide reducatase (RNR) is the key enzyme responsible for the biosynthesis of deoxribonucleotides, the building blocks for DNA. In RNR, a thiyl radical is made in order to reduce the ribose via hydrogen atom abstraction, a critical step for DNA biosynthesis.[12, 13, 14] Class I RNR in E. coli utilizes long-range electron transfer from a cysteine in one subunit, and occurs over ~ 35 Å to the tyrosyl radical in a second subunit, allowing the thiyl radical to take a hydrogen from the ribose and proceed with synthesis of the deoxyribonucleotide. In fact, both long-range electron transfer as well as proton-coupled electron transfer have been explored in RNR.[15]

1.3 Proton-coupled electron transfer theory

In examining the long-range electron transfer via radical intermediates, the need to avoid high-energy intermediates is required for effective redox activity. In some enzymes, this is achieved by what is known as proton-coupled electron transfer (PCET)

where electron transfer is coupled to proton transfer in order to circumvent high-energy ET processes from donor to acceptor. This concept of proton transfer influencing electron transfer has been an area of active research for several years.[16] Compared to individual ET processes, PCET is more complicated because both a proton and electron tunnel through a potential barrier. In doing so, the proton and electron influence each other thermodynamically and kinetically, where the motion of the proton affects H_{AD} as well as ΔG^o and λ. An example of PCET is found in photosystem II, where the TyrZ radical that was discussed previously undergoes oxidation by way of deprotonation to a nearby histidine.[2, 17] In this case, the electron can tunnel over much larger distances compared to the tunneling distance of a proton given the mass of a proton is 2000 times greater than that of an electron.

The key donors and acceptors for PCET reactions in proteins are amino acid radical intermediates, such as tyrosine, which may involve high-energy barriers. At physiological pH, the tyrosine cation radical, $Tyr^{\bullet+}$, has a very high oxidizing potential (E^o = 1.45 V vs. NHE) and low pK_a of -2, creating a thermodynamic barrier for the formation of this intermediate. Because of these thermodynamically unfavorable parameters, tyrosine proceeds to facilitate ET and PT by a concerted reaction mechanism.[2, 17] The drawback to a concerted mechanism is that a kinetic barrier involving proton motion is now introduced. In comparison, the tryptophan cation radical, $Trp^{\bullet+}$, exhibits a more accessible reduction potential (1.1 V vs. NHE) and pK_a (~4) in which case the formation of $Trp^{\bullet+}$ is a thermodynamically accessible

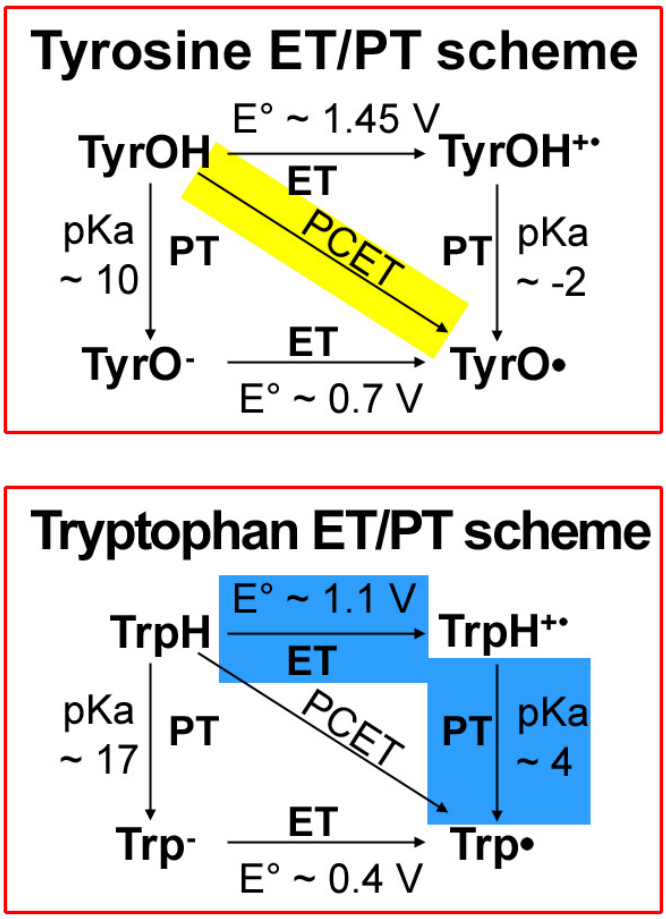

Figure 1.2: Electron and proton transfer schematics for tyrosine (top) and tryptophan (bottom). Reported thermodynamic parameters from tryptophan and tyrosine in solution[2] suggest that tyrosine likely undergoes PCET in cases of long-range electron transfer in proteins.

process and also avoids the kinetic barrier; therefore, ET/PT are observed as isolated events (Fig 1.2).[2,18]

1.4 Azurin as model protein for biological electron transfer

Large biomolecules such as photosystem II and ribonucleotide reductase are complex and difficult to study when attempting to understand long-range ET, amino acid radial intermediates, and PCET. To simplify these studies, the use of the model protein, *Pseudomonas aeruginosa* azurin, is used as a tool for studying ET between different amino acids as well as between residues and a metal center. [19, 20, 21] This 14 kDa protein is classified as a type I blue copper protein which has a characteristic ligand-to-metal charge transfer (LMCT) band at 628 nm (ε_{628} = 5900 M^{-1} cm^{-1}) and a Cu^{II} coordination sphere containing an axial methionine ligand (M121), a cysteine residue (C112), two histidines (H46 and H117), and a backbone carbonyl of a glycine residue (G45).[22] The native form of azurin contains two tyrosines (Y72 and Y108) and a single tryptophan located within the hydrophobic core of the protein (see Fig. 1.3). Upon oxidation and deprotonation of this native tryptophan, a distinctive neutral radical has been characterized spectroscopically and found to be relatively stable and long-lived. [20, 21] Azurin also displays astonishing chemical stability in various solvents and has been shown to withstand various mutations, making the protein an excellent model for studying ET pathways and amino acid radicals via site-directed mutagenesis and modulation of thermodynamic parameters.[19, 20, 21, 23]

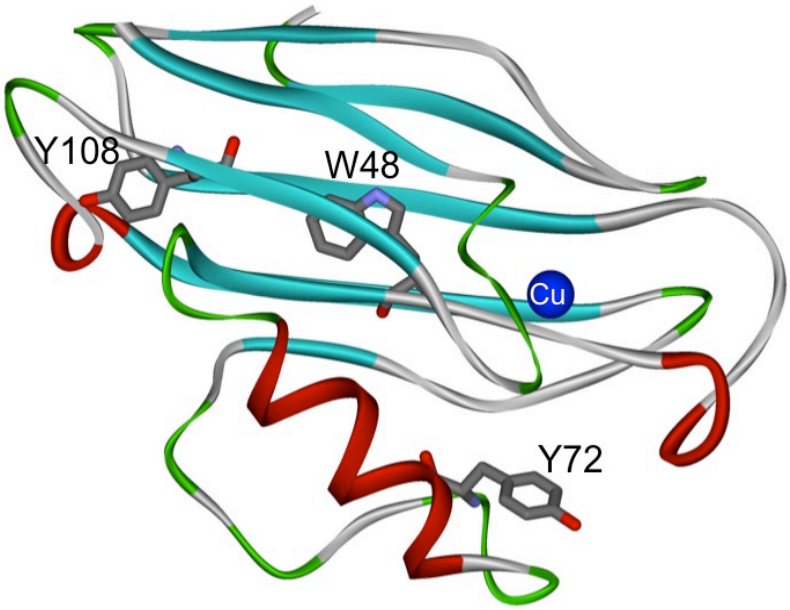

Figure 1.3: Crystal structure of WTaz (4AZU) showing native tryptophan and tyrosine residues as well as the copper site.

1.5 Nitrotyrosine as an unnatural amino acid in biomolecules

Unnatural amino acids such as fluorotyrosine, aminotyrosine, and nitrotyrosine are valuable tools for studying ET pathways in various proteins.[23, 24, 25] These specific tyrosine analogues are valuable in that all have phenolic p*K*a's that are within a physiological pH range of 5.6 to 8.4.[23] Substitution of tyrosine with these unnatural residues provides insight into ET pathways that are often unobservable because of the kinetic barrier to deprotonate tyrosine. For the case of Class I RNR where several native tyrosines are involved in electron hopping, modulation of pK_as also altered reduction potentials and gave information on tyrosine radical intermediates involved in the PCET mechanism.[25] Nitrotyrosine is particularly useful because of its absorption characteristics in the visible region. Fairly large extinction coefficients exist for both the phenol and phenolate at 360 nm and 430 nm, respectively, making the protein more easily monitored at various pHs for pK_a analysis, especially in the spectroscopically clear region of azurin's visible absorption spectrum (see Fig. 1.4). The use of nitrotyrosine in azurin is particularly valuable in studying tyrosine PCET due to the fact that both native tyrosines hold the possibility of quenching the previously reported photo-induced tryptophan cation radical.[20, 21]

The research reported in this thesis examines the thermodynamic properties of two natural tyrosines in azurin to investigate the electron transfer mechanism by which the well-characterized tryptophan radical in azurin is potentially quenched via PCET from tyrosine. To interrogate this reaction, several studies involving various exogenous molecules shed light on the mechanism of radical formation via electron ejection, where the neutral radical quantum yield is maximized upon photoexcitation of a zinc tyrosine-

free mutant in the presence of an irreversible electron quencher, $[Co^{III}(NH_3)_5Cl]^{2+}$. These optimized parameters for the generation of W48• provide a basis for studying ET from tyrosine to the tryptophan cation radical via steady-state absorption spectroscopy, as well as for examining the effectiveness of the unnatural amino acid, nitrotyrosine, in enhancing quenching events. Ultimately, these ET mechanisms in model protein azurin emphasize the importance of amino acids such as tyrosine and tryptophan in long-range electron transfer events.

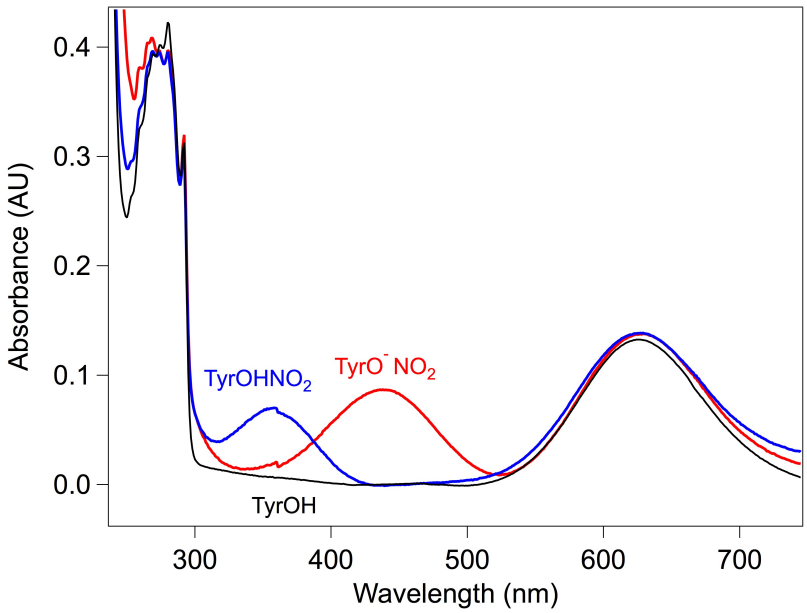

Figure 1.4: Absorption spectra of a single-tyrosine (Y72) azurin mutant with a single nitrated tyrosine at pH 4.5 (blue) and pH 8.7 (red).

2 Materials and Methods

2.1 Preparation of azurin protein

The preparation of azurin protein via site-directed mutagenesis, expression, and purification techniques has been outlined in the literature, and the following procedures are gathered directly from those resources.[19, 26] For conciseness, the methods are summarized below in order to aid future research studies and clarify any deviations from what has already been established as effective for the preparation of azurin protein.

2.1.1 Primer design and site-directed mutagenesis

Plasmid containing the azurin gene was donated from the groups of Prof. Harry Gray and Prof. John Richards at Caltech. To generate single amino acid mutations, primers were designed and ordered from Invitrogen (Carlsbad, CA) and DNA was amplified using polymerase chain reaction (PCR). Solutions were prepared via the QuikChange Site Directed Mutagenesis Kit (Stratagene, La Jolla, CA) and were heated and cooled in a thermal cycler (BioRad MJmini) according to the timing procedure in Table 2.1. Once amplified DNA was obtained, samples were then digested with DPN1 in the thermal cycler at 37ºC for 2 hours. PCR products were stored at -20ºC.

2.1.2 Transformation of PCR product

To obtain DNA for sequencing, PCR product was transformed into XL1-Blue Supercompetent cells that were provided with the QuikChange Site Directed Mutagenesis Kit. Under sterile conditions, 5 µL of PCR product was mixed with 25 µL of competent cells in sterile culture tubes. These tubes were then placed on ice for 5 minutes followed by 40 seconds of heat shock in a 42ºC bath. Following heat shock, 200 µL of sterile SOC

media (Table 2.2) was added to the tubes. Cells were then incubated at 37ºC with shaking at 180 RPM for 1.5 hours. After incubation, cells were plated on Luria broth (LB) agar plates with 70 mg/L ampicillin. Plates were inverted and incubated at 37ºC for 16 to 20 hours. Contents of agar plates and other media are described in Table 2.2.

2.1.3 Isolation of plasmid DNA

A single bacterial colony was picked from an agar plate and placed in 7mL of sterile LB media containing 70 mg/L ampicillin. Cells were incubated at 37ºC with shaking at 180 RPM for ~16 hours. DNA was extracted according to the protocol and solutions provided by QIAprep Miniprep DNA purification kit (Qiagen, Valencia, CA). Cells were pelleted at a centrifuge speed of 9, 000 RPM, and cell lysate was separated from large particulates at 14, 000 RPM for 30 seconds and 30 minutes, respectively. DNA purity was characterized by UV-vis absorbance at A_{260}:A_{280} (expected ratio = 1.80) and concentration was assessed at A_{260}. DNA was sequenced by Eton BioScience, Inc. (San Diego, CA).

2.1.4 Preparation of cell stocks

Once the desired mutation was confirmed, PCR product DNA was transformed into Invitrogen BL21 Star (DE3) competent cells following the steps described in section 2.1.2. A colony from the LB agar/ampicillin plate was picked and put in 5 mL of LB with 70mg/L ampicillin. Cells were incubated at 37ºC at 180 RPM for 16hrs, then spun down at 17,900 g for 10 minutes at 4ºC. Cells were re-pelleted in 2 mL of LB and 70 mg/L ampicillin. A few drops of sterile glycerol were added and cells were flash frozen before being stored at -80ºC.

Table 2.1: Thermal cycler method for PCR.

Step	Temperature (°C)	Time
1	95	30 sec
2	95	30 sec
3	55	1 min
4	68	5 min
5		Repeat steps 2-4, 12x
6	68	1 min
7	4	HOLD

Table 2.2: Recipes for microbiology media necessary for growth and expression of azurin protein. All media are brought to pH 7.0 with NaOH and HCl.

SOC Media	**1 L**
Tryptone	5 g
Yeast extract	5 g
NaCl	0.5 g
Water	965 mL
250 mM KCl	10 mL
2 M MgCl2	5 mL
Autoclave the above then separately add:	
1 M sterile glucose	20 mL

Luria broth (LB)	**1 L**
Tryptone	10 g
Yeast extract	5 g
NaCl	10 g
Water	1 L
For plates:	
Agar	15 g

Terrific broth (TB)	**1 L**
Tryptone	12 g
Yeast extract	24 g
Glycerol	4 mL
Water	900 mL
Separately make:	
Potassium phosphate, monobasic	2.31 g
Potassium phosphate, dibasic	12.54 g
Water	100 mL
Add phosphate solution to tryptone solution after autoclaving and cooling.	

2.1.5 Azurin protein expression

Expression of azurin begins by inserting a sterile pipette tip into a cell stock of interest to obtain a small amount of cells, and inoculating these cells in a 6 mL starter culture of TB media and 70 mg/L ampicillin. This culture is allowed to shake at 180 RPM at 37^{o}C for 8 hours. For a 6-12L growth of cells, media was prepared according to Table 2.2. Autoclaved phosphate solutions and yeast/bacto tryptone solutions were mixed after they cooled to room temperature, then 70 mg/L ampicillin was added to each shaker flask. The starter culture was inoculated into the 6-12 L of media, and cells were shaken at 37^{o}C for 16 hours at 180 RPM. After 16 hours, each 6 L flask of cells was induced with 1mL of 2mM β-D-1-thiogalactopyranoside (IPTG), then continued to shake for 4 additional hours. The cell growth was centrifuged at 5000 RPM for 5 min at 4^{o}C (1.5 L at a time), and the cell pellet was washed with 10 mM Tris pH 7.8 before storing at -80^{o}C. The average cell pellet was generally 25 grams per 6 L of growth.

2.1.6 Lysis of cells to isolate azurin protein

To separate azurin protein from other cell matter, cell pellets were thawed then mixed with ~ 50 mL of 20 mM potassium phosphate pH 7.2 per 25 g cell pellet. Approximately 200 mg of lyophilized hen egg lysozyme (USB Corporation, Santa Clara, CA) was added to this solution in addition to 40 μL of RNAse free DNAse I (Roche 10 units/ μL). Cell solution was stirred and allowed to lyse for 90 minutes, after which the lysis solution was placed into 25 mL bottles and centrifuged at 9500 RPM for 30 minutes at 4^{o}C. The supernatant was separated from the pellet, and brought to 50 mM sodium acetate pH 4.3 using a 1 M sodium acetate stock, and to 20 mM $CuSO_4$ by adding solid copper sulfate. Azurin is stable at this low pH, but other proteins precipitate from the

solution. The precipitated, unwanted proteins are removed via centrifugation at 5000 RPM for 15 min. The resulting lysate was stored in the fridge for up to a week at a time before exchanging into appropriate buffer for column purification. During this week, the solution changed color from light blue to dark blue, indicating that copper had been incorporated into azurin.

2.1.7 FPLC purification of copper azurin

After the cell pellet was lysed and copper sulfate was allowed to mix with the protein for a week, lysate was concentrated and exchanged with 20% ethanol using a 50 mL Amicon Ultrafiltration Cell with a 3000 NMWL YM membrane (Millipore, Billerica, MA). This step causes additional proteins to precipitate from the solution, and these precipitates are removed via centrifugation. After exchanging in ethanol, the lysate was exchanged into 1 mM sodium acetate, pH 4.5 for purification on a fast-protein liquid chromatography (FPLC) system (Amersham Biosciences, Piscataway, NJ). To separate azurin from cytochrome proteins, a 15-mL column of Source 15S cation-exchange beads was used (Amersham Biosciences, Piscataway, NJ). The column was equilibrated with 1 mM and 300 mM sodium acetate buffer, pH 4.5 according to Table 2.3, after which the crude protein was loaded and eluted over a 100 mL gradient of 1 to 300 mM acetate buffer, pH 4.5. Sample was collected in 2 mL fractions, and all blue fractions were assessed using absorption spectroscopy (Agilent 8430). Zinc azurin, which is clear, is the primary impurity at this stage. Because copper (II) azurin has a distinctive absorption band at 628 nm, a comparison of the relative amounts of zinc azurin and copper (II) azurin could be made based on the ratio of the 628 nm peak (from copper azurin only) and absorption of all aromatic residues at 280 nm (from copper and zinc azurins).[27]

Table 2.3: Equilibration method for FPLC System.

Total volume (mL)	FPLC Function	Value
0	Conc. Of buffer B (%)	0
0	mL/min	2
0	cm/mL	0.5
0	Valve position	1.3
25	Conc. Of buffer B (%)	0
25	Conc. Of buffer B (%)	100
50	Conc. Of buffer B (%)	100
50	Conc. Of buffer B (%)	0
50	Valve position	1.1
100	Conc. Of buffer B (%)	0
100	Conc. Of buffer B (%)	100
150	Conc. Of buffer B (%)	100
150	Conc. Of buffer B (%)	0
250	Conc. Of buffer B (%)	0
250	Alarm	0.2
250	Hold (Load protein)	
250	Port set	6.1
250	Conc. Of buffer B (%)	0
260	Conc. Of buffer B (%)	0
360	Conc. Of buffer B (%)	100

After this column purification step, the protein samples contain 30-60% zinc(II) azurin because of the relative abundance of zinc versus copper in the cells and media during expression. Experimental A_{280}:A_{628} ratios were calculated and compared to theoretical ratios determined from tyrosine ε_{280} of 1490 $M^{-1}cm^{-1}$, tryptophan ε_{280} of 5500 $M^{-1}cm^{-1}$, and Cu(II) azurin ε_{628} of 5900 M^{-1} cm^{-1} in pH 4.5 buffer. [27, 28] All azurin mutants and spectroscopic ratios for Cu(II) azurin discussed in this thesis are indicated in Table 2.4.

Table 2.4: Azurin samples and mutations with theoretical and experimental spectroscopic ratios for determining purity of Cu^{II} Az.

Azurin mutation	Notation	No. of Tyr.	No of Trp.	Residues in positions of native Y72, Y108, and W48	Theoretical ratio[a], $\varepsilon_{280}/\varepsilon_{628}$	Experimental ratio[a] $\varepsilon_{280}/\varepsilon_{628}$
Cu^{II} wild-type	CuWT	2	1	Y72, Y108, W48	1.3-1.4	1.6-1.7
Cu^{II} Y108F/Y72F	CuW48	0	1	F72, F108, W48	0.93	1.1-1.2
Cu^{II} Y108F/48W	CuY72	1	1	Y72, F108, W48	1.1-1.2	1.4-1.6
Cu^{II} Y72F/48W	CuY108	1	1	F72, Y108, W48	1.1-1.2	1.4-1.6
Cu^{II} Y72F/Y108F/ W48F	CuFFF	0	0	F72, F108, F48	0.22[b]	0.55[b]
Zn^{II} WTaz	ZnWT	2	1	Y72, Y108, W48	-	-
Zn^{II} 48W	ZnW48	0	1	F72, F108, W48	-	-
Zn^{II} Y108F/48W	ZnY72	1	1	Y72, F108, W48	-	-
Zn^{II} Y72F/48W	ZnY108	1	1	F72, Y108, W48	-	-
Zn^{II} Y72F NO_2/48W	ZnY108NO_2	1	1	F72, Y108NO2, W48	-	-
Zn^{II} Y108F NO_2/48W	ZnY72 NO_2	1	1	Y72NO2, F108, W48	-	-
Zn^{II} F110Y/48W	ZnF110Y	1	1	Y72, Y108, W48, Y110[c]	-	-

[a]Theoretical spectroscopic ratios are based on tyrosine ε_{280} of 990 $M^{-1}cm^{-1}$ (see section 2.3.3) or 1490 $M^{-1}cm^{-1}$, tryptophan ε_{280} of 5500 $M^{-1}cm^{-1}$, and ε_{628} of 5900 $M^{-1}cm^{-1}$ at pH 4.5.[27]

[b]Theoretical and experimental ratios for CuFFF were based on $\varepsilon_{260}/\varepsilon_{6280}$ and phenylalanine ε_{260} of 143 $M^{-1}cm^{-1}$.[29]

[c]Native residue in position 110 is F.

2.1.8 Potassium cyanide dialysis of azurin

Azurin exhibits strong binding affinities for several metals, including copper and zinc. $Cu^{II}Az$ can be dialyzed with cyanide to remove all metals, including copper and zinc, and reconstituted with a metal of choice to achieve higher purity samples.[30] The procedure used in our lab was adapted from a procedure described by Dr. Kyle M. Lancaster at Caltech (now at Cornell).[31]

First, the post-FPLC azurin sample was injected into a 7000 MW dialysis cassette and dialyzed against 500 mL of a solution that contained 100 mM potassium phosphate pH 8.0 and 400 mM potassium cyanide. Within 5 minutes, the blue color characteristic from the 628 nm ligand-to-metal charge transfer band disappeared, as seen in Figure 2.1. The sample was dialyzed in this solution twice for 4 hours each before removing the cyanide with 500 mL of 100 mM potassium phosphate pH 8.0 three times for 4 hours each. At this point, azurin could be re-metalated with zinc or copper by dialyzing the sample into 10 mM Tris buffer pH 7.5 for 4 hours followed by 10 mM Tris buffer pH 7.5 with 9 mM copper sulfate of zinc sulfate two times for 4 hours each. Take note that if greater than 10 mM of copper sulfate or zinc sulfate was added, zinc or copper hydroxide would crash out of solution and ruin the dialysis cassette. Also, given the danger of cyanide, all dialysis procedures should be performed in the hood.

The final sample of zinc or copper azurin was exchanged into 50 mM sodium acetate pH 4.5 and stored at 4^{o}C. To assess relative concentrations of copper and zinc, azurin samples were examined using inductively coupled plasma optical emission spectroscopy (ICP-OES) at the Scripps Institute of Oceanography (La Jolla, CA). Pure

Figure 2.1: $Cu^{II}Az$ dialyzing in 100 mM potassium phosphate, pH 8.0 and 400 mM potassium cyanide.

samples after potassium cyanide dialysis were generally 99:1 Cu:Zn or vice versa as assessed by this method.

2.1.9 Nitration of azurin

Nitration procedures were adapted from Dr. Crystal Shih and Dr. Brian Leigh.[32] Under nitrogen gas, 50 – 100 μM of 1 – 2 mM WT azurin and mutants that contain single tyrosine residues were nitrated in 8.5 mL of 100 mM potassium phosphate at a deprotonating pH of 12. After stirring under nitrogen gas for 15 min, a solution of 2% tetranitromethane (TNM) in 95% ethanol was added dropwise and a color change from blue to green was observed in copper azurin samples; a total of ~2 mL of this TNM solution was added. The nitration was allowed to stir under nitrogen gas and in the dark for 3 hours, after which the excess TNM was removed via an Amicon Ultrafiltration Cell, and the nitrated protein was exchanged into 50 mM sodium acetate pH 4.5. At low pH, copper azurin nitrotyrosine was a teal color while at high pH, the sample turned blue. Zinc azurin nitrotyrosine was yellow at low pH and colorless at high pH. These color changes are attributed to changes in protonation state of nitrotyrosine (discussed below).

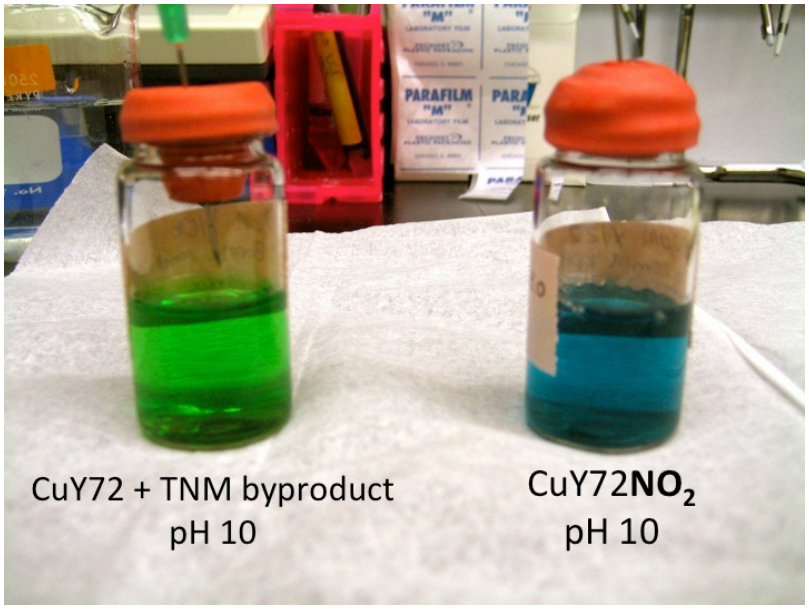

Figure 2.2: CuY72 and CuY72NO_2 in pH 10 after nitration with tetranitromethane. A successfully nitrated sample is teal at high pH (right) while an unsuccessfully nitrated sample is green (left) because of a mixture of TNM/ethanol byproduct and non-nitrated Cu^{II}Az.

2.2 Azurin sample preparation for spectroscopic experiments

2.2.1 Preparation of model NAYA and azurin samples for spectrophotometric titration

For spectroscopic titrations, 200 μL samples of 50 μM n-acetyl tyrosinamide (NAYA) and copper azurin were prepared in buffers ranging in pH from 7 to 13.5 in increments of approximately 0.25 pH units. For buffers within the range of 7 to 8.75 and 12 to 13.5, 100 mM potassium phosphate was used while 100 mM carbonate and 100 mM borate buffers were used for pH ranges 9 to 10.85 and 11 to 11.75, respectively. Samples were prepared using gas-tight syringes and those in pH 10 and below were prepared approximately 1 hour before obtaining a UV-vis spectrum (Shimadzu UV-3600). Samples above pH 10 were prepared a few minutes before measuring a spectrum.

2.2.2 Preparation of azurin samples for photolysis

Azurin samples prepared for photolysis ranged from 50 – 70 μM total protein in 20 mM potassium phosphate buffer pH 7.2. All samples were prepared in a round bottom flask attached to a 2 mm x 10 mm atmospheric quartz cuvette and were deoxygenated by attaching to a Shlenk line via a 24/40 ground glass joint and using nitrogen gas. The sample was subjected to 10 cycles of pump-purge, followed by stirring the sample for 5-10 minutes under gas while the vacuum re-equilibrated. This operation was repeated 5 times while a liquid nitrogen cooled trap captured any evaporated solvent. To compensate for solvent evaporation, excess solvent was added prior to deoxygenation, resulting in total sample volume before and after deoxygenating of ~ 1.3 mL and ~ 800 μL, respectively. Kontes valves formed a gas-tight seal that kept the cuvette deoxygenated for several hours.

External electron quencher molecules added to the samples included $Cu^{II}Az$, $Ru^{III}(NH_3)_6Cl_2$, and $[Co^{III}(NH_3)_5Cl]Cl_2$ and ranged in concentrations from 50 – 140 μM. A stock concentration of 2 mM $Ru^{III}(NH_3)_6Cl_2$ was used to prepare ~50 μM samples while 5 mM stock solutions of $[Co^{III}(NH_3)_5Cl]Cl_2$ were made fresh for each experiment given the $[Co^{III}(NH_3)_5Cl]^{2+}$ molecule irreversibly becomes $[Co^{II}(H_2O)_6]^{2+}$ when reduced.

2.3 Experimental instrumentation and calculations

2.3.1 Photolysis instrumentation and set-up

The neutral tryptophan radical at position 48 in azurin, W48•, was generated via direct photoexcitation using a CeraLux 175 W xenon arc lamp (LuxteL LLC, Danvers, MA). White light from the lamp was directed through a monochrometer set to 2.4 mm slit widths to create a 290 nm beam with a 10 nm bandpass. The atmosphere-controlled cuvette that contained sample was placed in a cuvette holder directly at the exit slit of the monochromator. To ensure that all 290 nm photons in the beam were passed through the sample, the cuvette was placed in the holder so that the beam was traveling along the 2 mm pathlength of the 2 mm x 1 cm cuvette. A microstir plate was placed below the beam path, and vertically along the cuvette on the side where the light was exiting. To ensure efficient stirring, the cuvette was gently shaken by hand approximately every 30 sec. The average power of the 290 nm light at the exit slit was 500-800 μW. An absorption spectrum was measured after every 3, 5, 10, and 15 min of total photolysis along the 1 cm pathlength on a UV-Vis-NIR spectrophotometer (Shimadzu UV-3600) where the spectral bandwidth was set to 1 nm. AzW48• radical absorption was determined by subtracting a pre-photolysis spectrum from each photolysis spectrum. Rates for the formation of

radical per minute were determined via a linear curve fitting of the OD_{515} per minute of photolysis.

2.3.2 Calculating tyrosine pK_as

Spectroscopic titrations were performed on single tyrosine mutants, CuY72 and CuY108, as well as CuWT. An absorption at 305 nm indicative of the tyrosinate mutant was plotted against pH and the titration curves were fitted via a non-linear least squares algorithm using Igor Pro V.6.0 to determine ε_{TyrO^-}, ε_{TyrOH}, and pK_as for each tyrosine. Equations for the single-tyrosine mutants and for WTaz are shown below.

Single-tyrosine curve fitting

$$f(pH)=C_{tot}\left[\frac{\left(\varepsilon_{YO^-}^{305}*10^{pH-pKa}\right)}{\left(1+10^{pH-pKa}\right)}+\varepsilon_{YOH}^{305}-\varepsilon_{YOH}^{305}\frac{\left(10^{pH-pKa}\right)}{\left(1+10^{pH-pKa}\right)}\right] \quad (2.1)$$

where C_{tot} is the total protein concentration, and ε_{YOH}^{305} and $\varepsilon_{YO^-}^{305}$ are extinction coefficients for tyrosine and tyrosinate at 305 nm, respectively.

Double tyrosine curve fitting

$$f(pH)=C_{tot}[\frac{\left(\varepsilon_{Y_{108}OH}^{305}*10^{pH-pK_aY_{72}}\right)}{\left(1+10^{pH-pK_aY72}\right)}+\varepsilon_{Y_{72}OH}^{305}-\varepsilon_{Y_{72}OH}^{305}\frac{\left(10^{pH-pK_aY_{72}}\right)}{\left(1+10^{pH-pK_aY_{72}}\right)}$$

$$+\varepsilon_{Y_{108}O^-}^{305}\frac{\left(10^{pH-pK_aY_{108}}\right)}{\left(1+10^{pH-pK_aY_{108}}\right)}+\varepsilon_{Y_{72}O^-}^{305}-\varepsilon_{Y_{72}O^-}^{305}\frac{\left(10^{pH-pK_aY_{108}}\right)}{1+10^{pH-pK_aY_{108}}}] \quad (2.2)$$

where C_{tot} is the total protein concentration, and $\varepsilon_{Y_{108}OH}^{305}$, $\varepsilon_{Y_{72}OH}^{305}$, $\varepsilon_{Y_{108}O^-}^{305}$, and $\varepsilon_{Y_{72}O^-}^{305}$ are extinction coefficients at 305 nm for indicated species. The pK_a values for CuY72 and CuY108 are indicated as pK_aY_{72} and pK_aY_{108}, respectively.

2.3.3 Calculation of tyrosine and nitrotyrosine ε_{280}

To determine the extinction coefficient at 280 nm of tyrosine and nitrotyrosine in azurin, known peak extinction coefficients of tryptophan and tyrosine (5500 $M^{-1}cm^{-1}$ and 1490 M^{-1} cm^{-1}, respectively) were used.[27] Subtraction of the absorption spectra of single-tyrosine azurin mutants (e.g. CuY72 or CuY108) from WT azurin spectra allowed us to isolate the absorption spectrum of the single tyrosine residue in the protein (e.g. Y72 or Y108). The resulting tyrosine spectra were found to be red-shifted from model compound n-acetyl tyrosinamide (NAYA). Given this observation, the $\boldsymbol{\varepsilon_{280}}$ of tyrosine in azurin was calculated to be 34% lower than that of NAYA, or 990 M^{-1} cm^{-1}. The extinction coefficient of nitrotyosine in azurin at 280 nm was also reduced by this amount, decreasing from 5830 M^{-1} cm^{-1} to 3850 M^{-1} cm^{-1}.[33]

2.3.4 Calculation of W48• quantum yields

Quantum yield calculations were derived by dividing the number of neutral tryptophan radicals generated by the number of excited tryptophan molecules (W48*) created (Eqn. 2.3). To determine the number of radical molecules generated, the concentration of closed-shell tryptophan after maximum photolysis time was used to derive the extinction coefficient of the radical at 515 nm; this was done assuming that the depletion of [Trp] was equal to the increase in [Trp•] (see Section 4.3). A post-photolysis absorbance value at 515 nm was multiplied by this extinction coefficient (ε_{515}) as well as sample volume (V) and Avogadro's number (N_a) to give the number of generated Trp• molecules (Eqn. 2.4).

To determine the number of excited tryptophan molecules, the number of photons absorbed was calculated using Beer's law, where the number of photons absorbed is the

difference between incident (I_0) and transmitted photons (I) (Eqn. 2.5). Transmitted light as a fraction of incident light was calculated based on the absorbance of the closed-shell tryptophan at 290 nm (Eqn. 2.5). We used the well known extinction coefficients of aromatic amino acids at 280 nm, but photolyzed at 290 nm in order to avoid tyrosine excitation; Eq. 2.5 converts the extinction at 280 nm to the photolysis wavelength of 290 nm. Incident laser power was between 550-800 μW and the excitation pathlength was 2 mm. Extinction coefficients for determining concentrations of protein, quencher, and radical are recorded in Table 2.5.

$$QY = \frac{\#\ Trp\bullet}{\#\ Trp^{*}} \tag{2.3}$$

$$\#\ Trp\bullet = [Trp\bullet]\ x\ (N_a)\ x\ (V) \tag{2.4}$$

$$[Trp\bullet] = \frac{A_{515}}{\varepsilon_{515}\ell}$$

$$\#\ Trp^{*} = \#\ \text{photons abs.} = I_0 - I = I_0 - I_0\left(10^{-\varepsilon\ell c}\right) \tag{2.5}$$

$$\varepsilon\ell c = A_{290} = \varepsilon_{280}\ell[Az]\ x\ \frac{A_{290*}}{A_{280}}$$

where A_{290*} is the absorbance with contribution from 280 nm protein absorbance

Table 2.5: List of relevant extinction coefficients used to calculate protein and quencher concentrations.

Residue/Quencher	λ (nm)	ε (M^{-1} cm^{-1})
Cu^{II}	628	5900
W48	280	5500
W48+Y	280	6490
WT	280	7480
$W48+YNO_2$	280	9350
$[Co^{III}(NH_3)_5Cl]^{2+}$	280	940
$[Ru^{III}(NH_3)_6]^{2+}$	280	300

[a]Based on tyrosine ε_{280} of 990 $M^{-1}cm^{-1}$ (see section 2.3.3) and tryptophan ε_{280} of 5500 $M^{-1}cm^{-1}$.

2.3.5 Potassium ferrioxalate actinometry

In order to accurately determine the number of photons emitted from the lamp source, a potassium ferrioxalate actinometric system was used following standard protocols.[34, 35] Briefly, a 500 μL solution of 0.006 M potassium ferrioxalate in 0.05 M H_2SO_4 was irradiated in a 2 mm by 10 mm cuvette with approximately 800 μW of 290 nm light. Irradiation times ranged from 1-2 min and the solution was shaken by hand every 30 seconds while being mixed with a stir bar. A 200 μL aliquot of this irradiated solution was added to 800 μL of 0.1 % phenanthroline in 0.5 M H_2SO_4 before collecting an absorption spectrum. The absorbance at 510 nm was measured and a calculated quantum yield of the ferrous ions was compared to a known quantum yield of 1.24 for 290 nm excitation.[34, 36] The actinometry results indicated that the power measured by our power meter should be divided by a factor of 1.04 for all W48• quantum yield calculations.

3 pK_as of native tyrosines

3.1 Introduction

Long-range electron transfer has been identified in several biological systems and has been shown to involve aromatic amino acids as radical intermediates.[37, 38, 39] In particular, tyrosine has been known to participate in multistep ET in the concerted deprotonation and oxidation process, PCET, [17] which is largely driven by thermodynamic parameters such as pK_as and redox potentials. The coupled deprotonation and oxidation of tyrosine effectively avoids high energy intermediates, however protein-derived PCET mechanisms remain poorly understood due to the complex hydrogen bond networks that can influence tyrosine's local environment.[40, 41, 42]

This motivation as well as previous studies from our group involving the native tryptophan neutral radical lead to the study of the native form of Cu^{II}Az, which has two tyrosines at positions 108 and 72 and a single-tryptophan at position 48.[20] Because tyrosine is often a critical redox-active participant in other biological systems and because the native tryptophan and its neutral radical in azurin have already been studied,[20,21] we aimed to investigate whether the tyrosine residues were participating in the redox chemistry of azurin. As a starting point, we focused on the thermodynamics of the tyrosine residues and the role of the protonation state on PCET reactions.

Typically, it is a challenging task to study PCET pathways in proteins because of the difficulty that is associated with modulating the hydrogen bonds that largely influence the proton transfer component. Unnatural amino acids have been implemented for several years in order to gain insight on the presence of ET and PCET reactions in different

systems.[25, 43, 44, 45, 46] Here, in order to observe possible PCET, the unnatural amino acid, nitrotyrosine, was used to analyze the possible role of tyrosine PCET on formation of the tryptophan neutral radical. Deprotonated nitrotyrosinate has a slightly higher reduction potential (1.07 V vs. NHE)[32] than that of deprotonated tyrosine and tryptophan, however exhibits a lower pK_a than that of tyrosine, making the residue an excellent probe for possible PCET reactions because the PT and ET reactions are decoupled.[25] These decreased pK_a values of Y108NO_2 and Y72NO_2 would not only allow deprotonation at a biologically feasible pH, but may also help generate a tyrosyl radical that is less sensitive to the hydrogen-bonding structure of the protein environment. Finally, for the case of azurin, nitrotyrosine is spectroscopically convenient because it absorbs at ~360nm while nitrotyrosinate absorbs at ~430nm, both of which are wavelengths that have essentially no absorbance in the native protein.

3.2 Materials and methods

3.2.1 Preparation of model NAYA and azurin samples for spectrophotometric titration

For spectroscopic titrations, 200 μL samples of 50 μM n-acetyl tyrosinamide (NAYA) and copper azurin were prepared in either 100 mM carbonate, borate, or phosphate buffer ranging in pH from 7 to 13.5 as discussed in section 2.2.1. Absorption spectra were collected using a UV-vis spectrophotometer (Shimadzu UV-3600).

3.2.2 Calculating tyrosine pK_as

Spectroscopic titrations were performed on the single-tyrosine mutants, CuY72 and CuY108, as well as CuWT. An absorption at 305 nm indicative of the tyrosinate mutant was plotted against pH and the titration curves were fitted via a non-linear least

squares algorithm using Igor Pro V.6.0 to determine ε_{TyrO-}, ε_{TyrOH}, and pK_as for each tyrosine. See equations 2.1 and 2.2 for the single-tyrosine mutants and for WTaz.

3.3 Results

3.3.1 Titration of tyrosine residues; structural basis for anomalously high pK_a values

When studying tyrosine radical intermediates in biological systems**,** thermodynamic parameters such as reduction potentials and pK_as help understand the propensity for tyrosine to participate in PCET.[17] Previously, our group studied spectroscopic characteristics of the native tryptophan, W48, via direct photoexcitation and the generation of a long-lived neutral radical, W48•. Further data suggested the possibility that Y108 could be redox-active, reducing the tryptophan cation radical, $W48^{\bullet+}$. This hypothesis is supported by the fact that there are reasonable ET paths between the tyrosine and tryptophan residues, and Y108 is 8.8 Å away from W48 while Y72 is 14.5 Å from W48 (Fig. 3.1). Observations of partially quenched neutral radical in the native species of azurin support the hypothesis that there is tyrosine-to-tryptophan ET.

To shed light on the thermodynamics of tyrosine and the residue's potential for facilitating ET to $W48^{\bullet+}$, pK_as for both tyrosine residues (Y72 and Y108) were obtained using UV-Vis absorbance spectrophotometric titrations on the mutants CuY108 and CuY72 as well as the native CuWT. Titrations were performed from pH 7.0 to pH 13.5. Above pH 10.0, spectral features in the far UV indicated that the protein was beginning to unfold, however features within the 290 nm to 700 nm region provided the relevant information to determine pK_a values. An increase in absorbance at 305 nm indicated the

formation of tyrosinate with increasing pH (Fig 3.2). A titration curve of Y108 indicated a pK_a of 13.32 ± 0.07 while a curve for that of the Y72 indicated a pK_a of 11.59 ± 0.03. A double tyrosine titration curve for WT indicated two pK_as of 11.01 ± 0.14 and 12.60 ± 0.08 for Y108 and Y72, respectively. Representative data are shown in Figure 3.2. These values can be compared to that of N-acetyl tyrosinamide, where a similar titration exhibited a pK_a of 9.8 ± 0.04.

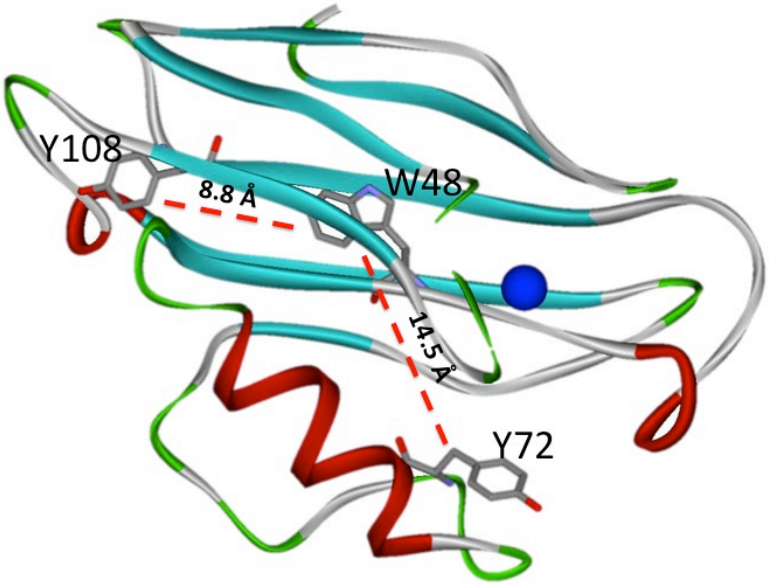

Figure 3.1: WTAz, which contains one tryptophan (W48) and two tyrosines, Y108 and Y72, which are 8.8 Å and 14.5 Å away, respectively. PDB ID: 4AZU

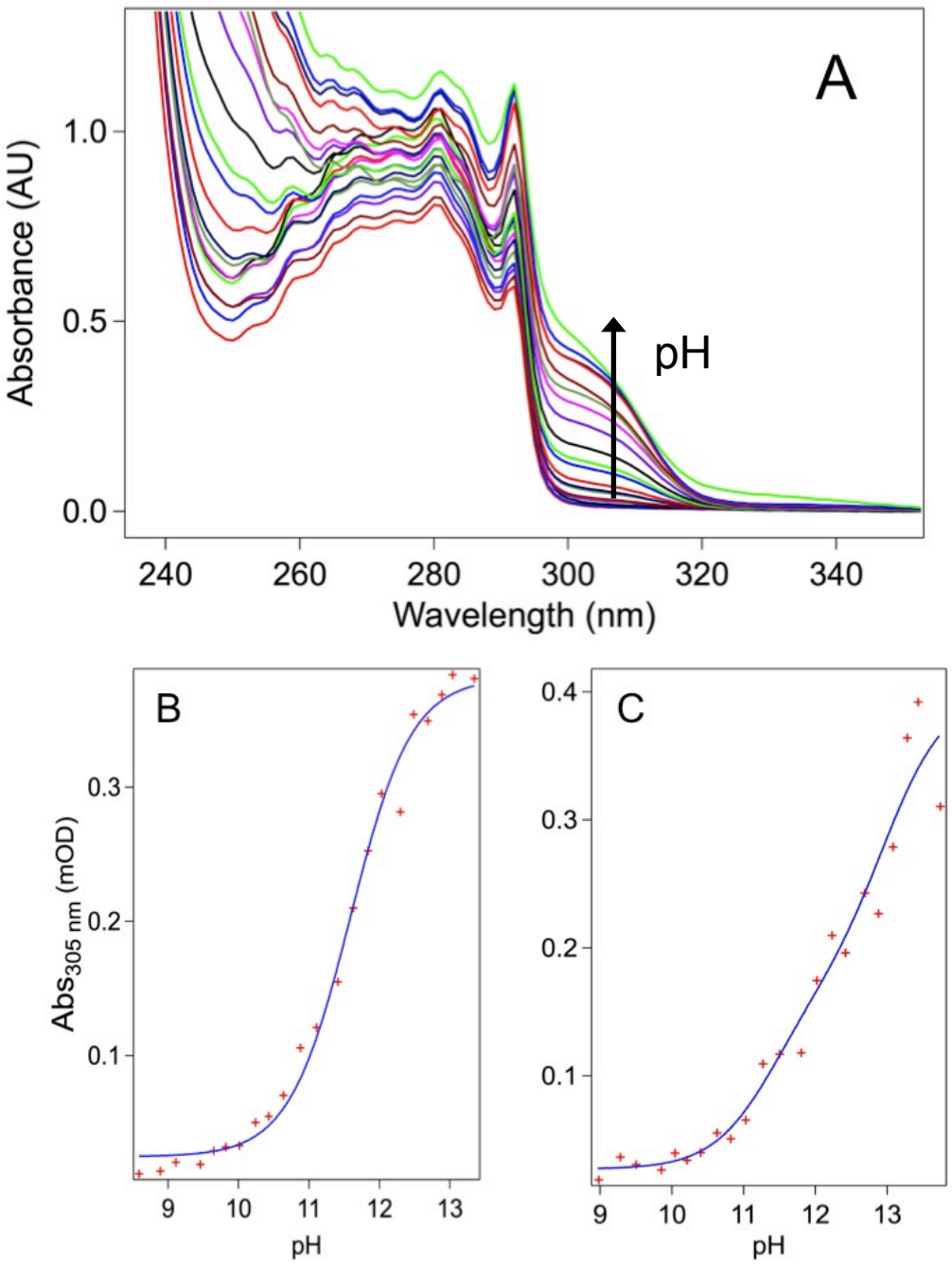

Figure 3.2: (A) Increase in tyrosine phenolate absorbance at 305 nm with increasing pH from pH 7 to pH 13.5 for CuWT. The absorption data at 305 nm as a function of pH was fit to Equations 2.1 and 2.2 for (B) single-tyrosine azurin mutant in panel A, and (C) WT.

3.3.2 MD simulation studies of single-tyrosine mutants

Given these unusually high pK_a values in the protein, the local environments of Y72 and Y108 were examined via crystal structure analysis (4AZU). Tyrosine at position 108 has the higher pK_a, and analysis of crystal structure indicates that a nearby glutamate residue (E106) could act as a hydrogen bond acceptor and thus allow facile tyrosine oxidation (Fig. 3.3). On the other hand, if the tyrosine residue is localized to a hydrophobic environment or near an anion, deprotonation may not be favored because of electrostatics.

To further examine the Y72 and Y108 environments, Pat Blachly from Prof. J.A. McCammon's group at UCSD performed constant pH molecular dynamics simulations on CuWT, as well as the single-tyrosine mutants, CuY108 and CuY72, over 10 ns.[47] This type of molecular dynamics simulation allows protonation states to change as various conformations are sampled. At the conclusion of the constant pH molecular dynamics simulation, the system has sampled a Boltzmann distribution of protonation states, allowing for calculation of pK_a values for the residues that titrated during the simulation. In each of the simulations, pK_as > 13 were calculated for both Y72 and Y108, and the orientation of E106 is pointed out towards solvent, contradicting the crystal structure orientation (Fig. 3.4). When E106 is pointing inward towards Y108, a lysine (K103) accompanies this movement and creates a salt bridge with E106. The local environment around Y72 indicates minimal charged residues and a slightly larger solvent exposure of the phenol than that of the solvent exposure of Y108. These factors likely contribute to the lower pK_a that is observed for Y72. The observation of E106 interacting with lysine

rather than Y108 and the overall hydrophobic environments of both tyrosines is consistent with the reported high pK_a values.

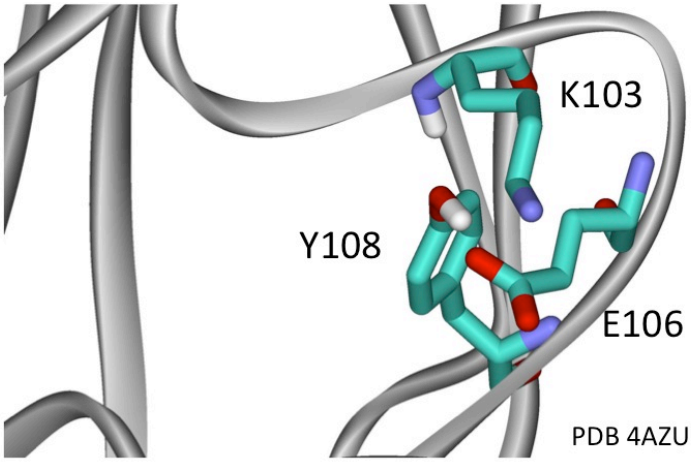

Figure 3.3: Protein environment near Y108 in WTaz. In the crystal structure (PDB 4 AZU), the carboxylate group of the nearby glutamate106 residue is pointed toward the phenolic hydrogen of tyrosine, acting as a proton acceptor. Alternatively, a nearby lysine103 residue may act as the H-bond donor with glutamate106.

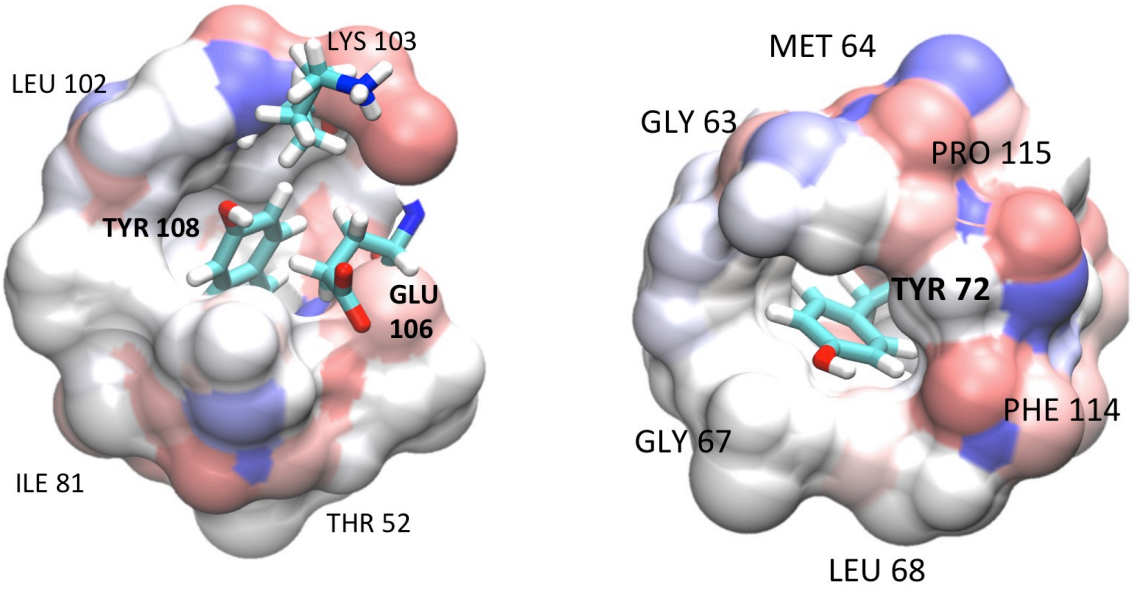

Figure 3.4: Molecular dynamic simulation results, courtesy of Pat Blachly from the lab of Professor J. Andrew McCammon. The images illustrate hydrophobic environments of Y108 (left) and Y72 (right). For the case of Y108, lysine points inwards to form a salt bridge with E106 in the brief periods when E106 is buried in the protein.

3.3.3 Titration of nitrated copper single-tyrosine mutants

To decrease tyrosine pK_as and further investigate possible PCET reactions, CuWT and single-tyrosine mutants were nitrated using tetranitromethane. Labeling yields on samples of CuY72, CuY108, and CuWT were between 30% and 50% using a NO_2Y^- ε_{430} of 4290 $M^{-1}cm^{-1}$ and a Cu^{II} LMCT ε_{628} of 5900 M^{-1} cm^{-1}.[25, 28] These yields were satisfactory for performing spectroscopic titrations where, with increasing pH, the absorption of the phenol decreased at 360 nm concomitant with an increase in the absorption of the phenolate at 430 nm. An isosbestic point is expected to appear at 393 nm, but is affected by baseline variations, as shown in Fig 3.5. Titrations were performed from pH 4.5 to 10.5 and absorbance values at 360 nm and 430 nm were plotted against pH and fit to Equation 3.1 Curve fittings yielded pK_as of 8.91 ± 0.12 and 6.71 ± 0.07 for $Y108NO_2$ and $Y72NO_2$, respectively (Fig. 3.6), which were approximately 3.5 and 4.8 pH units below the pK_as of non-nitrated CuY108 and CuY72. In addition, the pK_a of $Y72NO_2$ is in fact relatively close to the pK_a of 7.0 for nitrotyrosine in solution.[48] The biologically feasible pK_a values for both tyrosines suggest the possibility of decoupled electron and proton transfer despite the limits of hydrophobic environments.

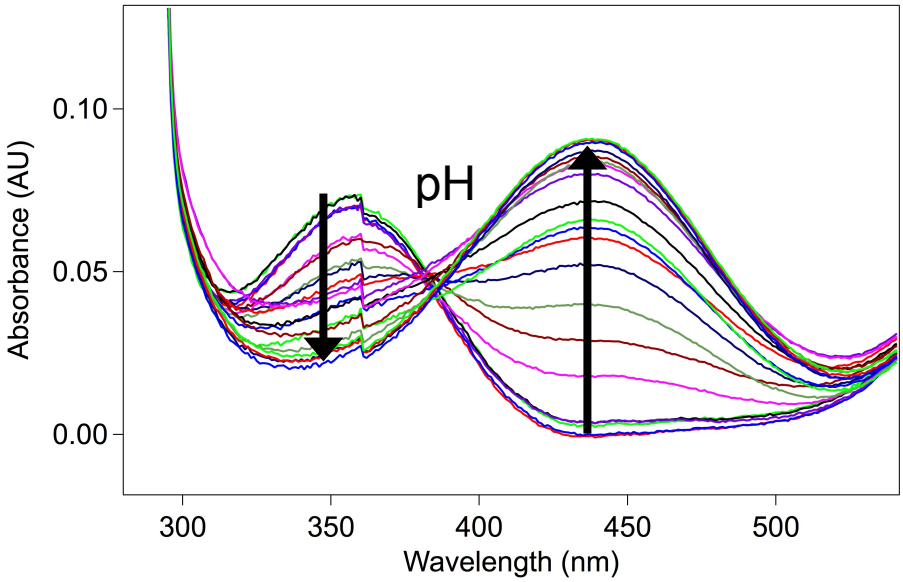

Figure 3.5: Spectrophotometric titration of nitrotyrosine. As the pH increases, the absorption of the phenol at 360 nm decreases concomitant with an increase in the absorption of the phenolate at 430 nm. An isosbestic point is expected at 393 nm.

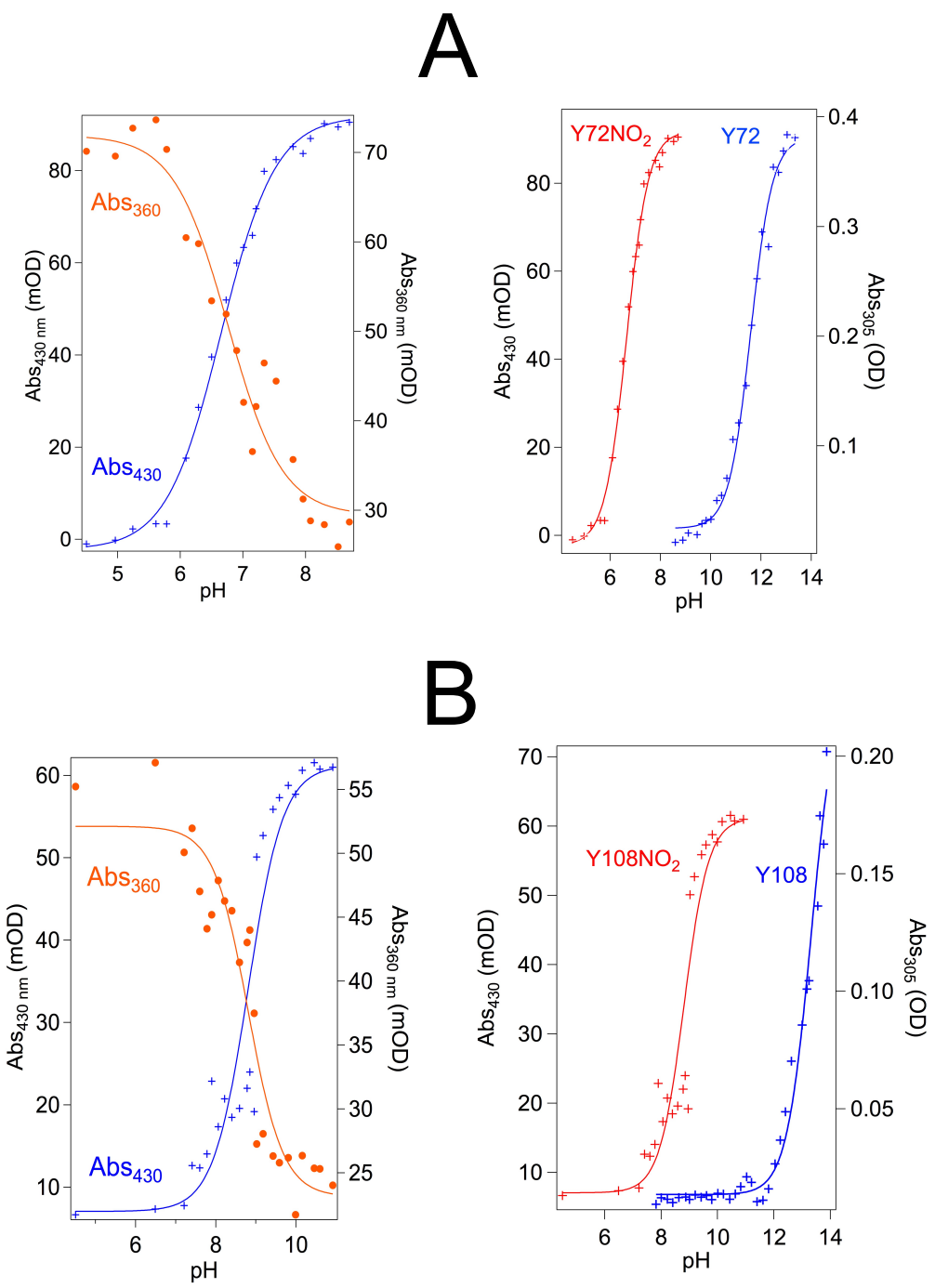

Figure 3.6: Comparison of spectrophotometric titration curves for (A) $Y72NO_2$ and (B) $Y108NO_2$. Absorbance data at 360 nm and 430 nm as a function of pH were fit to equation 2.1. An average of the two pK_as found from 360 nm and 430 nm resulted in a pK_a of 6.71 for $Y72NO_2$ and a pK_a of 8.91 for $Y108NO_2$.

3.4 Discussion

The use of aromatic amino acid side chains as a mediator for long-range electron transfer is a commonly investigated topic of research, and for the case of tryptophan and tyrosine, radical intermediates are generated in these long-range ET events. The reduction potentials for tryptophan and tyrosine in model compounds have been previously studied, and both the neutral and cation tryptophan radicals have been found to have greater reduction potentials than tyrosine at pH 7.[2] For tyrosine specifically, the pK_a of the phenol has been shown to have a critical influence on the residue's reduction potential.

In protein systems, PCET reactions involving tyrosine are often dictated by hydrogen bonding and the relative hydrophobicity of the tyrosine environment.[49] Using a small, natural protein system, the possibility of tyrosine PCET was investigated by analyzing pK_a thermodynamic parameters and examining environments via molecular dynamic simulations. Anomalously high pK_a values were found for both Y108 and Y72, indicating high thermodynamic barriers that could be inhibiting PCET at a biologically feasible pH. Other studies of the native tyrosine pK_as in azurin have utilized natural abundance ^{13}C NMR spectroscopy and fluorescence spectroscopy.[50, 51] Those studies indicated pK_as of 11.4 and 10.75 for Y72, and 12.5 and 12.78 for Y108 using each method, respectively.

Effects of protein environment and hydrogen bonding on tyrosine pK_a are complicated but have been observed in previous studies. For instance, a high pK_a value for a tyrosine residue in ribonucleotide reductase (Y122) was observed and is consistent with our results, where an aspartate resides in the local environment of the Y122, thereby disfavoring the charged tyrosinate.[25] A native tyrosine in *Rh. Sphaeroides* has also shown

fluctuations in pK_a with protein environment, where the replacement of a nearby histidine with glutamate subsequently increased the tyrosine pK_a by 2 units. In this case, the negatively charged carboxylate group on glutamate likely acts as a hydrogen bond acceptor and prevents ionization, an observation that has also been connected to a cytochrome *c* oxidase proton transfer pathway.[52, 53] In addition to the influence of local hydrogen bond acceptors, another contribution to the high pK_as is likely the hydrophobic pockets that surround both Y72 and Y108. For the case of tyrosine PCET, a hydrophobic environment would prevent the loss of a proton to solvent as well as destabilize a resulting anion; these conditions may favor the formation of a hydrogen bond between tyrosine and glutamate, which is consistent with a higher pK_a. An inverse correlation between pK_a and reduction potential has been reported for the case of tyrosine, suggesting a decrease in the reduction potential of Y108 relative to free tyrosine E°(Tyr•/TyrOH) = 0.93 V, pH 7.[2, 23, 25] On the other hand, the hydrophobic environment of W48 increases the reduction potential of $W48^{\bullet+}$ relative to model compounds (E°(TrpH•+/TrpH) = 1.02 V, pH 7),[2] further increasing the driving force for tyrosine ET to tryptophan. Ultimately, these observations of a high pK_a value and possible hydrogen bonding within a hydrophobic environment may serve to affect the driving force for PCET between either Y72 or Y108 and $W48^{\bullet+}$, however electrostatic considerations of local environments add uncertainty to this hypothesis.

Unnatural amino acids are commonly used in protein systems in order to investigate the influence of intramolecular environment. Nitrotyrosine in particular has proven to be an excellent probe for understanding how protein environment modulates pK_a and lowers the thermodynamic barrier that often inhibits PCET reactions.

Spectroscopic titrations indicated that both tyrosine pK_as in azurin were decreased by ~3.5 to 4 pH units when nitrated. In addition, both Y72NO_2 and Y108NO_2 are shown to have pK_as that are at a biologically feasible pH, where the pK_a of Y72NO_2 is in fact relatively close to the pK_a of 7.0 for nitrotyrosine in solution.[48] As will be discussed in Ch. 4, high quantum yields of the neutral tryptophan radical are reported when a tyrosine-free mutant, ZnW48, is mixed with an exogenous quencher $[Co^{III}(NH_3)_5Cl]^{2+}$ and photolyzed with 290 nm light. Preliminary direct photolysis experiments of the ZnY108 NO_2 mutant with the $[Co^{III}(NH_3)_5Cl]^{2+}$ quencher at pH 7.6 indicate a 3-fold decrease in yield of W48• relative to that generated in ZnW48 with the same quencher. These results indicate possible ET from Y72NO_2 to $W48^{\bullet+}$ at a deprotonating pH of 7.6. In contrast, at a pH below that of the pK_a (6.7), one would expect that the quantum yield for formation of the tryptophan radical is unaffected by the presence of a nitrated tyrosine.

Ultimately, the substantial decrease of both nitrotyrosine pK_as leaves room for further investigation of photoinduced PCET from nitrotyrosine even when there is a significant effect of protein environment on the reactivity of tyrosine radical intermediates. To further demonstrate the utility of nitrotyrosine, pH dependent photolysis studies are underway in order to reinforce the effect of decoupling proton and electron transfer and more clearly model charge transfer events over long distances within complex protein systems.

In conclusion, analysis of pK_as and local environments of native tyrosines in azurin has directed studies into electron transfer via amino acid radical intermediates. The reduction potentials for tryptophan and tyrosine in model compounds have been previously studied,[2] and in protein systems, these potentials are likely modulated by local

environment. For tyrosine specifically, the pK_a of the phenol has been shown to have a critical influence on the residue's reduction potential, where hydrogen bonding can influence tyrosine PCET capabilities.[49] If either Y108 or Y72 were redox active, this would allow for the study of possible proton-coupled electron transfer pathways involving coupled deprotonation of a native tyrosine to the reduction of $W48^{\bullet+}$.

4 Photolysis of zinc azurin in the presence of exogenous quenchers

4.1 Introduction

Amino acid radical intermediates are central to the study of biological electron transfer (ET) processes. Recently, our group reported a long-lived neutral tryptophan radical that was accompanied by reduction of Cu^{II} to Cu^{I} after 290 nm photoexcitation of the W48 residue in the tyrosine-deficient azurin mutant (CuW48). Initially, it was proposed that this stable neutral radical W48 was formed after an electron was transferred through the protein to the Cu^{II} center, followed by irreversible deprotonation of the initially formed tryptophan cation radical. The steady-state absorption spectrum revealed two peaks at 485 nm and 515 nm, which were indicative of the neutral species. A concomitant decrease in the 628 nm absorption was attributed to disappearance of the Cu^{II} ligand-to-metal charge transfer (LMCT) band.[21]

The yield of radical formation, $\Phi_{W48\bullet/W48*}$, was measured in CuW48, and the yield appeared are believed to occur simultaneously. Hence, the ease of proton release is expected to impact the efficiency for tyrosine-based PCET.

Despite extensive experiments that focused on the role of tyrosine in azurin redox chemistry, the mechanism for generation of tryptophan radical was still not confirmed. In fact, the initial proposal of intramolecular ET came into question as we performed additional experiments. Specifically, metal analysis via ICP-OES revealed that azurin samples contained a mixture of Cu^{II} and Zn^{II} azurins, with Zn^{II} species contributing 40-60% of the total protein; this range depended on sample preparation. This finding of

significant population of ZnAz motivates the current studies to investigate whether the tryptophan radical could be generated by ZnAz in the presence of an electron acceptor.

4.2 Materials and methods

4.2.1 Preparation and photolysis of azurin samples

Azurin samples prepared for photolysis ranged from 50 – 70 μM total protein in 20 mM potassium phosphate buffer pH 7.2. All samples were photolyzed under deoxygenating conditions as indicated in section 2.2.2. Direct photoexcitation was accomplished using a CeraLux 175 W xenon arc lamp (LuxteL LLC, Danvers, MA), where white light from the lamp was directed through a monochromator set to 2.4 mm slit widths to create a 290 nm beam with a 10 nm bandpass. The atmosphere-controlled cuvette that contained sample was placed in a cuvette holder directly at the exit slit of the monochromator and stirred via stir plate apparatus and by manually shaking every 30 seconds. Absorption spectra were collected using a UV-Vis-NIR spectrophotometer (Shimadzu UV-3600). W48• radical absorption was determined by subtracting a pre-photolysis spectrum from each photolysis spectrum and rates for the formation of radical per minute were determined via a linear curve fitting of the OD_{515} per minute of photolysis.

4.2.2 Calculation of W48• quantum yields

Quantification of the quantum yield is described in section 2.3.3. Briefly, radical quantum yield were determined by dividing the number of neutral tryptophan radicals generated by the number of excited tryptophans (W48*) created (Eqn. 2.3). To determine the number of radical molecules generated, a post-photolysis absorbance value at 515 nm was multiplied by this extinction coefficient (ε_{515}) as well as sample volume (V) and

Avogadro's number (N_a) to give the number of generated Trp• molecules (Eqn. 2.4).

To determine the number of excited tryptophan molecules, the number of photons absorbed was calculated using Beer's law, where the number of photons absorbed is the difference between incident (I_0) and transmitted photons (I) (Eqn. 2.5). Transmitted light as a fraction of incident light was calculated based on the absorbance of the closed-shell tryptophan at 290 nm (Eqn. 2.5).

Radical yields are reported along with a standard deviation.

4.2.3 Potassium ferrioxalate actinometry

Actinometry is described in section 2.3.4. Results from actinometry experiments indicated that the readings from our power meter should be divided by a factor of 1.04.

4.3 Results

4.3.1 Photolysis of ZnW48 and CuAz

The cause for high radical yields in samples that contained a mixture of ZnAz and CuAz was probed by photolysis of isolated, pure ZnW48 and CuW48 as well as their mixtures. Samples of pure ZnW48 produced no radical when photolyzed (see Fig. 4.1). This result was also observed with the photolysis of pure CuW48 (Fig 4.1). The lack of radical in pure CuW48 was an unexpected finding that led to the conclusion that presence of ZnW48 contributed considerably to the formation of the tryptophan neutral radical in mixtures with CuW48.

By systematically varying the concentrations of ZnW48 and CuW48 in a given mixture, we mimicked the impure samples that had been studied in the past and that had given rise to significant concentrations of W48•. Standard amounts of ZnW48 were added to a given concentration of pure CuW48 to monitor the change in radical yield as a

function of relative concentrations. Photolysis of a 2:1 mixture of ZnW48 and CuW48 resulted in a linear bleach as a function of time of Cu^{II} absorbance accompanied by an increase in absorption at 485 nm and 515 nm over 15 minutes, revealing an isosbestic point at 528 nm (see Fig. 4.2). To determine radical yields, W48• absorbance at 515 nm was recorded and calculated as discussed in Section 2.3.3. Resulting radical yields increased linearly with increasing ZnW48 concentrations up until a ratio of 1:1 ZnW48:CuW48. Similarly, an analysis of the change in radical yield upon addition of CuW48 to ZnW48 revealed increasing radical yield with increasing concentration of CuW48 up to a 1:1 ratio of ZnW48 and CuW48. The quantum yield for a 1:1 mixture was found to be 0.067±0.012 (Table 4.1). These findings indicate that the observation of high quantum yields in samples that contained ZnW48 and CuW48 could be attributed to intermolecular as opposed to purely intramolecular events.

Table 4.1: Summary of W48• quantum yields gathered after 15 minutes of total photolysis. The ratio indicates protein:quencher.

Az Sample	Quencher	Ratio	pH	$\Phi_{W48\bullet/W48*}$
ZnW48	none	1:1	7.2	0
$Cu^{II}W48$	none	1:1	7.2	0
ZnW48	$Cu^{II}W48$	1:1	7.2	0.067±0.012
ZnW48	CuFFF	1:1	7.2	0.057±0.003
ZnW48	$[Ru^{III}(NH_3)_6]^{2+}$	1:1	7.2	0.063±0.008
$Cu^{I}W48$	$[Ru^{III}(NH_3)_6]^{2+}$	1:1	7.2	0
$Cu^{I}W48$	$Cu^{II}W48$	1:1	7.2	0
ZnW48	$[Co^{III}(NH_3)_5Cl]^{2+}$	1:1	7.2	0.080±0.010
ZnW48	$[Co^{III}(NH_3)_5Cl]^{2+}$	1:2	7.2	0.087[a]
ZnW48	$[Co^{III}(NH_3)_5Cl]^{2+}$	1:4	7.2	0.093[a]
ZnW48	$[Co^{III}(NH_3)_5Cl]^{2+}$	1:1	4.5	0.087±0.003
ZnW48	$[Co^{III}(NH_3)_5Cl]^{2+}$	1:1	9.0	0.064±0.004

[a]Photolysis experiments for these mixtures were performed only once.

We hypothesized that the intermolecular mechanism is one that involved photo-ejection of an electron, followed by quenching of this ejected electron by $Cu^{II}W48$. This hypothesis was further studied with $Cu^{I}W48$, which, like ZnW48, contains a d^{10} metal center that cannot be further reduced. A sample of $Cu^{II}W48$ was mixed with $Cu^{I}W48$ and photolyzed, and the change in the Cu^{II} LMCT absorbance at 628 nm was monitored. In this mixture, the expectation is that radical would be produced because of electron ejection from $Cu^{I}W48$ while the LMCT band would decrease because of electron capture by the Cu^{II} species; this is the behavior that was observed for the ZnW48 and $Cu^{II}W48$ mixtures. The observation was not consistent with this expectation. Over 25 minutes, the absorbance at 628 nm increased to 33% of the expected A_{628} if all the Cu^{I} protein were to be converted to Cu^{II} with no W48• radical production. This increase may reflect electron ejection directly from the Cu^{I} metal to form the Cu^{II} species, or fast intramolecular ET from Cu^{I} to the transient tryptophan cation radical. The latter possibility is consistent with the observation of no tryptophan radical and increased LMCT band.

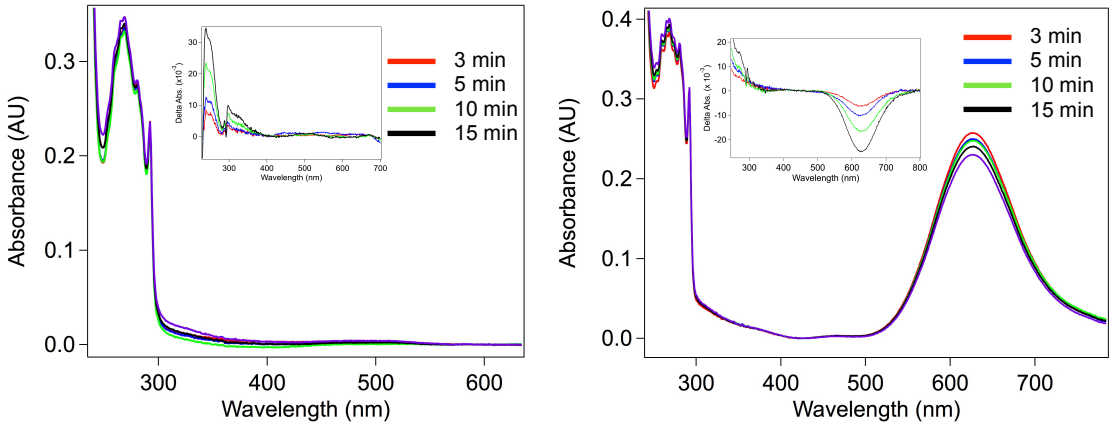

Figure 4.1: Absorption spectra of ZnW48 (left) and $Cu^{II}W48$ (right) in 20 mM phosphate buffer pH 7.2 collected over 15 minutes of photolysis time. *Insets*: Difference absorption spectra of ZnW48 and $Cu^{II}W48$ photolysis, respectively.

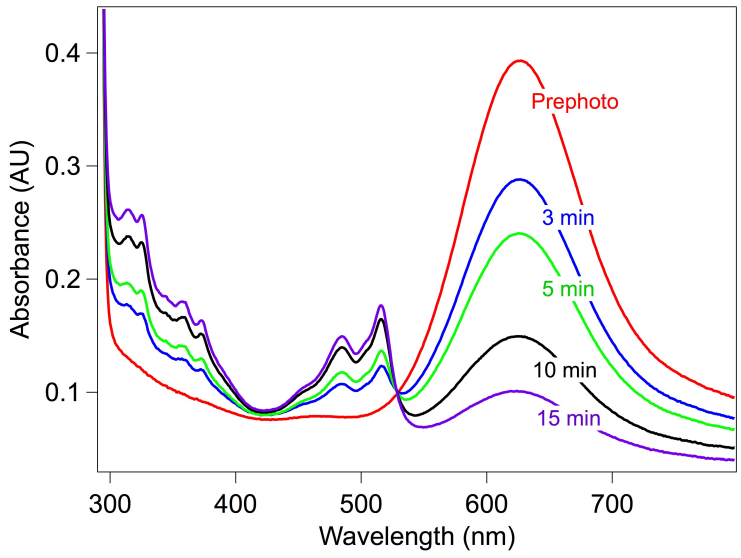

Figure 4.2: Absorption spectra of 1:2, CuW48:ZnW48 in 20 mM phosphate buffer pH 7.2 collected over 15 minutes of photolysis time.

A mixture of ZnW48 and a tyrosine-free and tryptophan-free mutant, CuFFF, was also photolyzed to compare with the behavior to Cu^{II}W48 quencher. The purpose of this mixture was to eliminate the possibility that the W48 species in Cu^{II}W48 was participating in the photochemistry. A quantum yield of 0.057 ± 0.003 was calculated after photolysis of this mixture, while a mixture of ZnW48 with CuW48 resulted in a quantum yield of 0.067 ± 0.012. These values are very similar, and indicate that in mixtures of ZnW48 and Cu^{II}W48, the radical is generated nearly entirely in the ZnW48 mutant, not in Cu^{II}W48.

4.3.2 Photolysis of ZnW48 and CuW48 with $Ru^{III}(NH_3)_6Cl_2$ exogenous quencher

Given the results of radical formation upon systematic addition of a Cu^{II}W48 as the exogenous electron quencher, other known electron scavengers were used to further analyze the ET event associated with formation of the tryptophan neutral radical. A reversible oxidative quencher, $Ru^{III}(NH_3)_6Cl_2$, was added to individual samples of pure ZnW48 and pure CuW48. Upon photoexcitation, an ejected electron from W48 is expected to be scavenged by the exogenous quencher, resulting in reduction of $[Ru^{III}(NH_3)_6]^{2+}$ to form $[Ru^{II}(NH_3)_6]^{2+}$. $[Ru^{III}(NH_3)_6]^{2+}$ was added in a 1:1 ratio to ZnW48, which is a similar ratio in studies of the ZnW48:CuW48 mixtures, resulting in a radical quantum yield of 0.063 ± 0.008. This yield is comparable to the value obtained for the ZnW48:CuW48 ($\Phi_{W48\bullet/W48*}$ = 0.067 ± 0.012).

In comparison to experiments on the Cu^{II}W48/Cu^{I}W48 mixture, $[Ru^{III}(NH_3)_6]^{2+}$ was also utilized as an external quencher. We first added this exogenous quencher to a sample of Cu^{I}W48 (1:4 Cu^{I}W48 : $[Ru^{III}(NH_3)_6]^{2+}$) in order to observe oxidation of Cu^{I}.

The results of this experiment were slightly unexpected, given that the oxidation of Cu^{I} to Cu^{II} was only 10% of the maximum expected Cu^{II} absorbance after 115 minutes (Figure 4.3). This conversion of 10% was surprisingly similar to that of the 1:1 Cu^{I}:Cu^{II} mixture, which we discussed above in section 4.2.1. We also investigated mixtures of Cu^{II}W48 and $[Ru^{III}(NH_3)_6]^{2+}$ and found that no radical was generated in this mixture, nor were they any observed changes in the LMCT band beyond that which could be attributed to generic photodestruction of protein by the UV light.

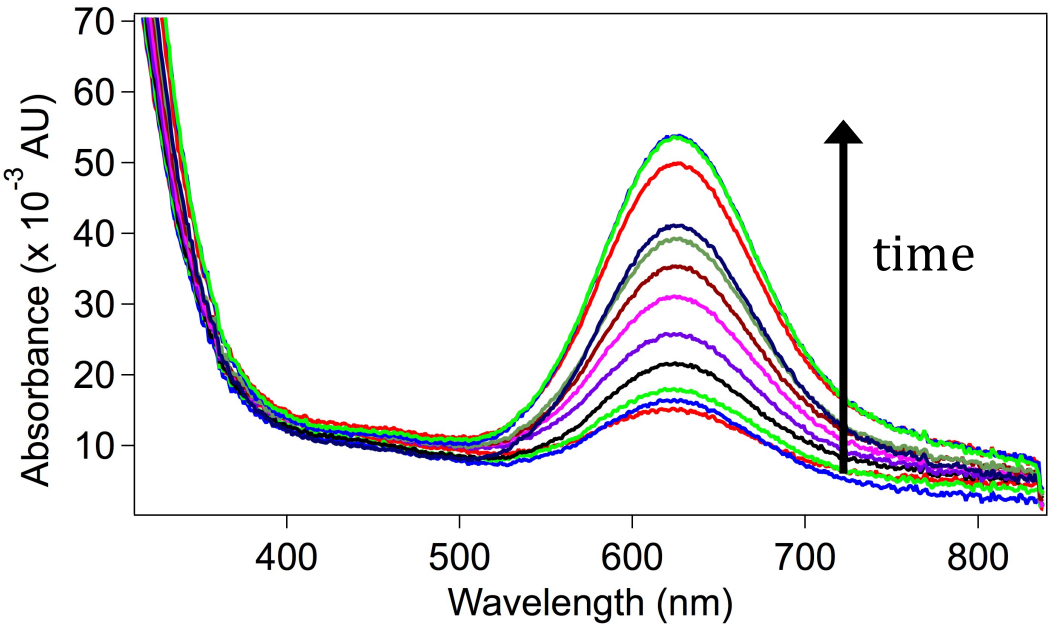

Figure 4.3: Absorption spectra of 1:4, $Cu^{I}W48$: $[Ru^{III}(NH_3)_6]^{2+}$ in 20 mM phosphate buffer pH 7.2 collected over 40 minutes of photolysis time. The maximum amount of Cu^{II} that could be generated would correspond to absorption of 0.30.

4.3.3 Photolysis of ZnW48 and CuW48 with $[Co^{III}(NH_3)_5Cl]^{2+}$ exogenous quencher

Another molecule commonly used as an exogenous electron scavenger is $[Co^{III}(NH_3)_5Cl]^{2+}$. The advantage of this quencher relative to the CuAz and Ru-based quenchers is that reduction of $[Co^{III}(NH_3)_5Cl]^{2+}$is irreversible, thereby shutting down further redox chemistry. In these experiments, a maximum absorbance of the tryptophan neutral radical at 515 nm was observed. Absorbance peaks at 485 nm and 515 nm increased linearly with time from 0 to 15 minutes. A slope of the absorbance at 515 nm minutes was determined for each sample, and this change in absorbance was used to determine the amount of radical made per second and compare to the amount of excited tryptophan made per second.

When Cu^{II}W48 was photolyzed in the presence of $[Co^{III}(NH_3)_5Cl]^{2+}$, there was no indication of radical formation in the visible region (see Fig. 4.4). However, there was a reproducible increase in absorption between 250 and 400 nm, but we have not identified the molecular origin of this increase. The decrease at 235 nm represents the decrease in absorption of $[Co^{III}(NH_3)_5Cl]^{2+}$ as it is reduced to $[Co^{II}(NH_3)_5Cl]^{2+}$. A small decrease in absorbance at 628 nm was also observed, however, it is unclear whether this is directly from tryptophan-mediated electron transfer or from another electron transfer event; this decrease is typically seen after photolysis of every tryptophan containing sample, with or without an electron scavenger, and may also represent destroyed protein.

In comparison, when ZnW48 is photolyzed in the presence of $[Co^{III}(NH_3)_5Cl]^{2+}$, a decrease in the spectroscopic features between 230 nm and 300 nm is observed, with an

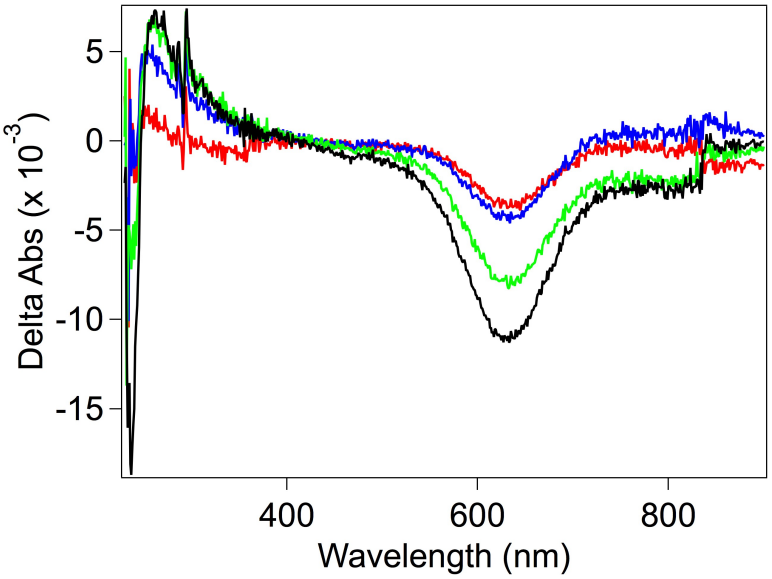

Figure 4.4: Difference absorption spectra of 1:1 mixture of $Cu^{II}W48$ and $[Co^{III}(NH_3)_5Cl]^{2+}$ in 20 mM phosphate buffer pH 7.2.

increasing absorbance of the characteristic radical peaks at 325 nm, 360 nm, 485 nm, and 515 nm. Both $[Co^{III}(NH_3)_5Cl]^{2+}$ and closed-shell tryptophan absorb strongly between 220 nm and 280 nm; decreases in absorbance at these wavelengths reflect loss of tryptophan because of conversion to the radical as well as reduction of Co^{III} to Co^{II} (see Fig 4.5). A decrease in absorbance at these UV wavelengths is apparent in the ZnW48 and $[Co^{III}(NH_3)_5Cl]^{2+}$ mixtures, and this result contrasts with experiments on the Cu^{II}W48 and $[Co^{III}(NH_3)_5Cl]^{2+}$ mixture, suggesting minimal reduction of $[Co^{III}(NH_3)_5Cl]^{2+}$ from Cu^{II}W48 is occurring and the ET for reforming the closed-shell tryptophan is unclear.

The ZnW48 species was further studied by adding systematic amounts of $[Co^{III}(NH_3)_5Cl]^{2+}$. When ZnW48 was mixed with $[Co^{III}(NH_3)_5Cl]^{2+}$ in a 1:1 ratio, a radical quantum yield of 0.080 ± 0.010 was obtained, which is 0.017 units above value of the radical quantum yield obtained with a 1:1 ratio of ZnW48 and $[Ru^{III}(NH_3)_6]^{2+}$ mixture. Photolyzing a mixture of 1:2 ZnW48: $[Co^{III}(NH_3)_5Cl]^{2+}$ resulted in a radical quantum yield of 0.087, while a ratio of 1:4, ZnW48: $[Co^{III}(NH_3)_5Cl]^{2+}$ gave an only slightly higher quantum yield of 0.093. Because the absorbance increased linearly with time only up to 15 minutes, all quantum yields were based on the slope of this absorbance per minute up to 15 minutes. The slope of radical absorption as a function of time remained positive at longer times, but the slope was reduced after 20 minutes of total photolysis (see Fig 4.6). Though the decreasing rate of radical formation is not fully understood, it may reflect the balance between radical formation and radical decay since the lifetime of the radicals is on the order of hours. In our experiments, a maximum

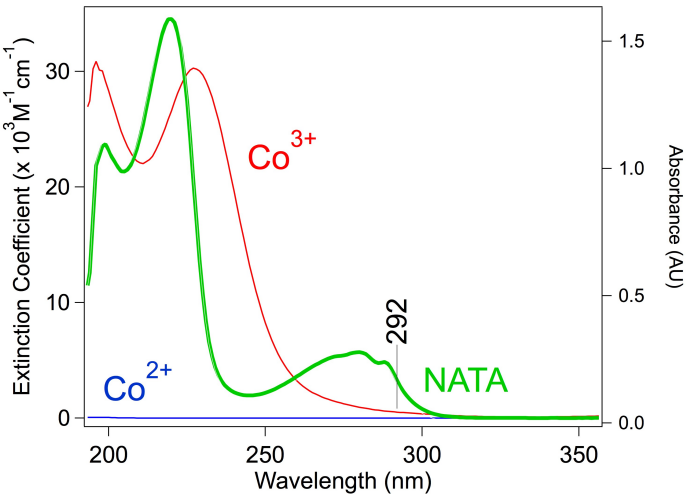

Figure 4.5: Absorption spectra of 50 µM $[Co^{III}(NH_3)_5Cl]^{2+}$ and 50 µM $[Co^{II}(NH_3)_5Cl]^{2+}$ in 20 mM phosphate buffer pH 7.2 illustrating minimal absorption at 292 nm. A spectrum of the model compound N-acetyl-tryptophanamide (NATA) is shown for comparison.

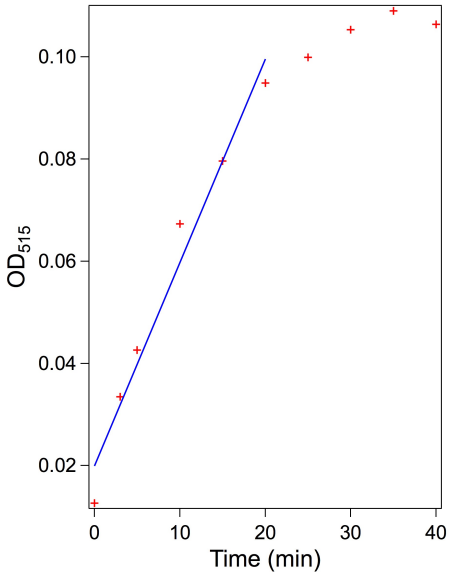

Figure 4.6: Absorbance of W48• at 515 nm vs. time from photolysis of 1:1, ZnW48 : $[Co^{III}(NH_3)_5Cl]^{2+}$.

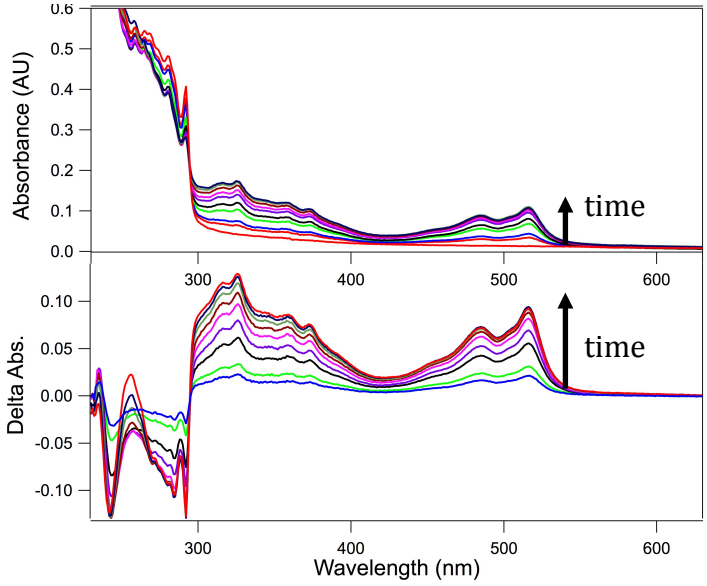

Figure 4.7: Top panel: Absorption spectra of 1:1, ZnW48 : $[Co^{III}(NH_3)_5Cl]^{2+}$ in 20 mM phosphate buffer pH 7.2 collected over 40 minutes of photolysis time. Bottom panel: Difference absorption spectra to highlight radical peaks. The spectra are the result of post-photolysis – pre-photolysis spectra, shown in the top pane.

absorbance at 515 nm was achieved at 35 minutes of photolyzing ZnW48 and $[Co^{III}(NH_3)_5Cl]^{2+}$ (see Fig. 4.7).

4.3.4 Photolysis of ZnW48 and CuW48 with N_2O

N_2O is a commonly used solvated electron scavenger and was utilized to saturate samples of ZnW48, Cu^{II}W48, and a mixture of both species.[54, 55] If the mechanism of formation of W48• involves photoejection of a solvated electron, we would expect that N_2O would scavenge this electron so it could not reduce Cu^{II}. In the presence of N_2O, only the ZnW48+Cu^{II}W48 mixture generated W48•and there was no observable W48• when Cu^{II}W48 or ZnW48 was photolyzed in the presence of N_2O. The samples of Cu^{II}W48 and ZnW48+Cu^{II}W48 with N_2O showed ~10% and ~6% Cu^{II} LMCT bleach, respectively. It was surprising that ZnW48 in saturated N_2O solution did not generate W48• because we expected N_2O to act as a solvated electron scavenger. However, when Cu^{II}W48 and ZnW48 samples were individually mixed with $[Co^{III}(NH_3)_5Cl]^{2+}$ and N_2O, W48• absorbance was observed in the ZnW48 + $[Co^{III}(NH_3)_5Cl]^{2+}$ mixture only (Figure 4.8). In summary, for all samples photolyzed in the presence of N_2O in comparison to photolysis results without N_2O, no changes in the amount of W48• were observed. Additionally, the fact that N_2O showed different behavior as an electron scavenger than $[Co^{III}(NH_3)_5Cl]^{2+}$ or Cu^{II}W48 indicates that the situation is much more complex than a simple solvated electron mechanism. For example, it is possible that $[Co^{III}(NH_3)_5Cl]^{2+}$ and/or Cu^{II}W48 binds to ZnW48 such that an electron is not ejected to the solvent but instead, is quickly quenched by a scavenger that is non-specifically bound to ZnW48. Alternatively, it is possible that N_2O exhibits complex behavior as a solvated electron

scavenger in a protein solution, and/or N_2O quenches the cation radical via non-specific binding to the protein.

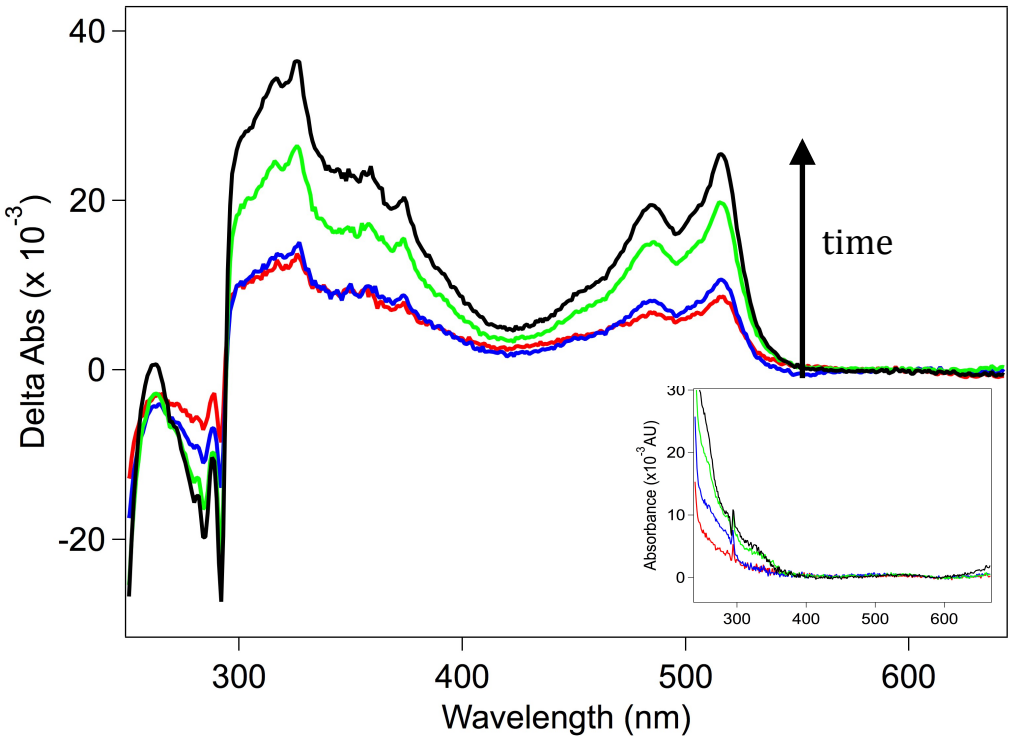

Figure 4.8: Difference absorption spectra of 1:1 ZnW48: $[Co^{III}(NH_3)_5Cl]^{2+}$ saturated in N_2O gas. The absorbance at 515 nm increases with time up to 15 minutes. *Inset*: Photolysis of ZnW48 saturated with N_2O.

4.3.5 pH dependent photolysis of ZnW48 with $[Co^{III}(NH_3)_5Cl]^{2+}$

Photolysis experiments involving the pH dependence on quantum yields were performed with a mixture of ZnW48 and $[Co^{III}(NH_3)_5Cl]^{2+}$. Previously, all photolysis procedures were performed at pH 7.2. Here, we photolyzed at pH 4.5 in order to examine the pH dependent quenching behavior of $[Co^{III}(NH_3)_5Cl]^{2+}$. At pH 7.2 (20 mM photassium phosphate buffer), photolysis samples contained ~ 50 μM ZnW48, ~50 μM $[Co^{III}(NH_3)_5Cl]^{2+}$, and ~0.1 μM H^+ while a pH 4.5 sample in 50 mM sodium acetate buffer contained ~ 50 μM ZnW48, ~50 μM $[Co^{III}(NH_3)_5Cl]^{2+}$, and ~30 μM H^+. Because aqueous H^+ will also scavenge solvated electron, the pH 4.5 sample contained up to ~1.7 times as much quencher than the samples at pH 7.2. Comparison of quantum yields indicated a slight, 0.007 unit increase for the pH-4.5 sample relative to that of the pH-7.2 sample. This increase can be compared to a similar increase of 0.007 units when the excess quencher is in the form of $[Co^{III}(NH_3)_5Cl]^{2+}$, i.e. for a 1:2 mixture of ZnW48 and $[Co^{III}(NH_3)_5Cl]^{2+}$. The trend of increased quantum yield with decreased pH is further supported by photolysis of ZnW48 and $[Co^{III}(NH_3)_5Cl]^{2+}$ at pH 9, where the quantum yield was reduced by 0.016 units relative to the photolysis of ZnW48 and $[Co^{III}(NH_3)_5Cl]^{2+}$ at pH 7.2. These results indicate that H_3O^+ may be a more effective scavenger than $[Co^{III}(NH_3)_5Cl]^{2+}$, and/or that there is a pH-dependence on the formation of the neutral tryptophan radical, most likely in the deprotonation of the cation radical. A comparison of all quantum yields with various quenchers is summarized in Table 4.1.

4.4 Discussion

Past analyses of the tryptophan radical revealed vital information on the role of protein environment on electron and proton transfer pathways via amino acid radical intermediates. The mechanism for tryptophan radical generation in azurin was previously discussed when CuW48 was believed to have made W48• without the presence of exogenous electron scavengers. However, the previous observation of increasing quantum yield with decreasing sample purity (purity based on A_{280}/A_{628}) led us to the current studies. To obtain higher purity samples, we expanded our sample preparation protocol where cyanide was used to remove all metals, including contaminants, followed by re-metallation with a metal of choice (Zn or Cu). In mixtures of highly pure CuW48 and ZnW48, an intermolecular ET reaction between CuW48 and ZnW48 became evident. The importance of the protein metal center and the presence of exogenous quenchers became evident with the photolysis of the tyrosine-deficient mutant of azurin and the observations are discussed below.

We have better resolved the issue of inter- vs intramolecular ET to generate the tryptophan radical. The initial hypothesis proposed that the ET pathway involved 290 nm excitation of tryptophan (W48*) that would directly transfer an electron to Cu^{II}; deprotonation of $W48^{\bullet+}$ would then generate the long-lived tryptophan neutral radical. The competition between the deprotonation rate and back-ET from Cu^{I} to the tryptophan radical was believed to control the quantum yield. These prior photolysis experiments were performed on samples that contained varied mixtures of Cu and Zn azurin.

After sample purification and photolysis of isolated and highly pure CuW48, no radical absorbance at 485 nm or 515 nm was observed. We believe that a likely reaction

is the photoejection of an electron from W48* in ZnW48 that reduces Cu^{II} in Cu^{II}W48 followed by deprotonation of $W48^{\bullet+}$. In a sample that contains pure CuW48 or a mixture of CuW48 and Co^{III} quencher, there is minimal Cu^{II} bleach, and no radical absorbance is observed. The lack of radical indicates that there is probably no photoejection of an electron in this mutant but rather the electron may pursue the thermodynamically feasible intramolecular route that was initially proposed. However, in this case, back-ET rate is very fast and re-reduces the transient tryptophan radical cation before deprotonation.[21]

Other possible intermolecular reactions became more evident upon mixing species of ZnW48 and CuW48. When mixed, Cu^{II} in CuW48 behaves as an intermolecular electron quencher, where upon photoexcitation, a large amount of neutral tryptophan radical as well as Cu^{I} is observed. This spectroscopic observation suggests that a dominating ET reaction involves reduction of Cu^{II} by the photoejected electron in mixtures of ZnW48 and CuW48, followed by deprotonation of the transient tryptophan cation radical in the ZnW48 species. In the zinc species, zinc cannot reduce the cation radical, therefore the tryptophan cation radical in the zinc species cannot be reduced by a metal center. With increasing concentrations of Cu^{II}W48, an increase in radical quantum yield reveals the electron quenching ability of the Cu^{II} species and supports intermolecular ET in a mixture of the CuW48 and ZnW48 species.

Given that Cu^{II}W48 could be used as an electron scavenger, this species was also used to analyze oxidation of Cu^{I} in Cu^{I}W48. Unlike zinc, copper (I) in azurin can reduce the tryptophan cation radical, which is evident with the rise in Cu^{II} LMCT absorbance at 628 nm. With increasing photolysis time, the Cu^{II} LMCT absorbance for a mixture of Cu^{I} and Cu^{II} increased while there was no W48• absorbance. In the Cu^{I}W48 sample, we

propose that $W48^{\bullet+}$ is rapidly reduced by Cu^{I}, which contributes to the increased absorbance at 628 nm because of generation of Cu^{II} as well as lack of neutral radical signal. In this scenario, we would theoretically expect the LMCT signal to be unchanged because the solvated electron is scavenged by Cu^{II} while the tryptophan cation radical is reduced by Cu^{I}; if the yields for each of these reactions were equivalent, the intensity of the LMCT band would stay constant. The fact that there is an increase in the LMCT band indicates that the yields are not equivalent, and/or there are other photoprocesses, such as direct electron ejection from Cu^{I}. The presence of $[Ru^{III}(NH_3)_6]^{2+}$ electron scavenger with $Cu^{I}W48$ increases the 628 absorbance as well (see Figure 4.3), supporting the notion that back-ET from Cu^{I} may be reducing the cation radical due to significant driving force and low reorganization energy.[21, 38] Therefore, photolysis of the $Cu^{I}W48$ species in the presence of an exogenous quencher does not generate W48• because the initial product, $W48^{\bullet+}$, may be quenched via ET from the metal center.

To further explore the photoejection process, the exogenous quencher, $[Ru^{III}(NH_3)_6]^{2+}$, was mixed with ZnW48. $[Ru^{III}(NH_3)_6]^{2+}$ is a common oxidative reversible quencher meaning the molecule can readily change oxidation states without decomposition. In this case, the ground state of the excited state tryptophan can be regenerated without damaging the system (Ru^{III}/Ru^{II} couple is 0.10 V).[56] Photolysis results of ZnW48 with $[Ru^{III}(NH_3)_6]^{2+}$ indicate similar radical quantum yields to those obtained from the ZnW48 mixture with CuW48. However, because $[Ru^{III}(NH_3)_6]^{2+}$ and $Cu^{II}W48$ undergo reversible redox chemistry, it was not clear if the radical yields were impacted by the reversible reactions.

Electron scavenging from excited state tryptophan was also investigated with the irreversible exogenous quencher, $[Co^{III}(NH_3)_5Cl]^{2+}$. In this molecule, the ammonia ligands dissociate upon reduction, irreversibly becoming $[Co^{II}(H_2O)_6]^{2+}$.[19] Photolysis of Cu^{I}W48 with $[Co^{III}(NH_3)_5Cl]^{2+}$ results in no steady-state radical generation in addition to no steady-state spectroscopic evidence of Cu^{II} or $[Co^{III}(NH_3)_5Cl]^{2+}$ reduction. In this case, the intermolecular electron transfer that may be occurring is similar to that suggested from observations of the Cu^{I}W48 and $[Ru^{III}(NH_3)_6]^{2+}$ mixture. Photoexcitation of W48 generates $W48^{\bullet+}$ that is immediately reduced by Cu^{I}. Though steady-state experiments cannot directly give evidence for a specific ET pathway, photolysis of Cu^{I}W48 with the reversible $[Co^{II}(NH_3)_5Cl]^{2+}$ ultimately suggests a quenched tryptophan cation radical.

Mixtures of $[Co^{III}(NH_3)_5Cl]^{2+}$ with ZnW48 resulted in the highest radical quantum yield observed and thus allowed for a more accurate calculation of the neutral radical extinction coefficient at 515 nm. A maximum concentration of W48• was observed after 40 minutes, suggesting that a correlation could be made between the maximum amount of W48• generated and the maximum amount of W48 converted to W48•. The closed-shell tryptophan absorption peak at 292 nm was removed by a scaled subtraction of the pre-photolysis spectrum, and this fraction was representative of the remaining closed-shell tryptophan (see Figure 4.9). This analysis indicated a maximum 70% conversion of W48 to W48•. With knowledge of the starting, pre-photolysis, concentration of ZnW48 of 55 μM, we could estimate an extinction coefficient of the neutral radical of ε_{515} of 2140 M^{-1} cm^{-1}. In this calculation, we have assumed that all closed-shell W48 that has been depleted was transformed to W48•; it is possible that a portion of W48 may undergo other photodestruction processes, so the extinction coefficient represents a lower limit,

and the actual extinction coefficient of the neutral radical is likely larger than 2140 M^{-1} cm^{-1}.

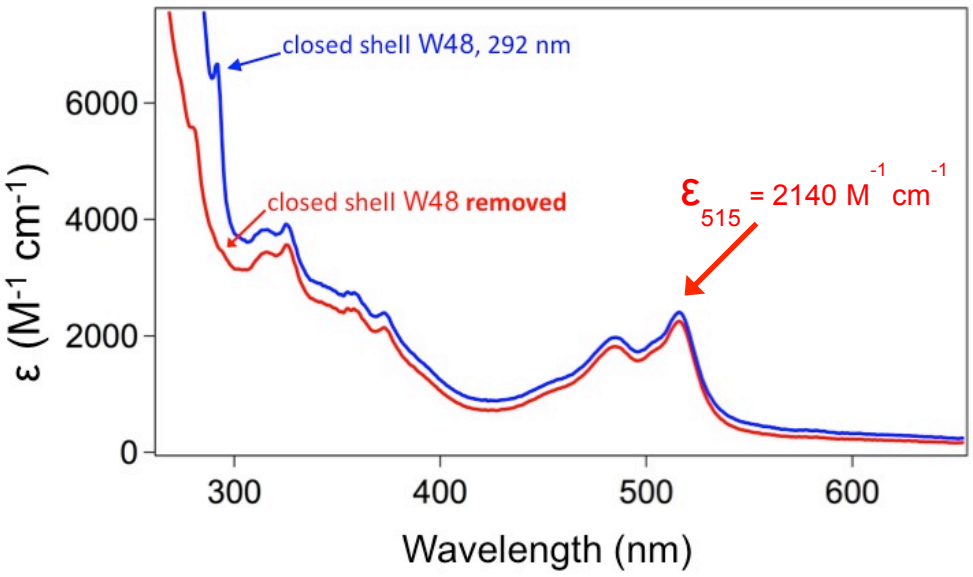

Figure 4.9: Absorption spectra of ZnW48 + $[Co^{III}(NH_3)_5Cl]^{2+}$ in a 1:2 mixture after 40 minutes of photolysis. The red spectrum is without any subtractions and the blue spectrum is with a scaled subtraction in order to remove the closed-shell W48 absorption peak at 292 nm.

In past studies, N_2O has been found to be a significant electron scavenger.[55] In our studies of N_2O with azurin, we would expect a steady-state buildup of tryptophan radical with N_2O as the scavenger; however, as reported previously, the lack of radical formation is unclear and we propose that association between N_2O and the protein matrix is quenching the cation radical.[21] Radical generation by other quenchers nonetheless supports electron ejection of the excited-state tryptophan via solvated electron.

The photoejection of an electron in the zinc tyrosine-deficient mutant was further probed by pH dependence studies. At various pH values, $[Co^{III}(NH_3)_5Cl]^{2+}$ exhibits Pourbaix behavior, where with increasing pH, the reduction potential decreases. In this case, at a lower pH, our results of a higher quantum yield are consistent with the expected increase in potential of $[Co^{III}(NH_3)_5Cl]^{2+}$ where the potential increases from 0.3 V to 0.462 V on going from pH 7.2 to 4.5. [19, 57] Furthermore, there is an increase in concentration of H^+ that also contributes to quenching of the solvated electron and therefore also results in to increased radical quantum yield. In fact, the effective quenching of H^+ relative to $[Co^{III}(NH_3)_5Cl]^{2+}$ is taken into consideration here where a greater quantum yield is observed for a lower pH ($[H^+]$ = 30 μM at pH 4.5). Despite the knowledge that the solvated electron is one of the most powerful reductants with a reducing potential of 2.77 V,[58] the effects of pH on the quenchers appear to be important. Our observations of increasing radical quantum yield with increasing pH in mixtures of ZnW48 and $[Co^{III}(NH_3)_5Cl]^{2+}$ further support the effective quenching of a photoejected electron.

Collectively, these studies involving different electron quenchers provide information on maximizing the radical quantum yield of W48• using an irreversible

quencher, and for directing studies toward ET mechanisms within a single molecule of azurin. Using different mutants of zinc azurin, we can now study how to quench the tryptophan cation radical by other residues such as tyrosine and more closely examine the influence of local environments on intramolecular ET.

5 W48• quenching studies

5.1 Introduction

Proton-coupled electron transfer (PCET) is a fundamental mechanism found in several biochemical systems. To accomplish long-range electron and proton transfer, nature has evolved to utilize amino acid radical intermediates, most notably via the aromatic residues, tyrosine and tryptophan. For example, photosystem II uses a tyrosine radical (TyrZ) to mediate ET across > 20Å.[59, 60] Charge transfer events between these radical intermediates can occur in a step-wise or concerted fashion; in nature, these events are more often concerted and occur on the microsecond time scale.[61] In the presence of a hydrogen bond, tyrosine PCET rates have been shown to increase by up to three orders of magnitude versus solvated proton rates.[62]

Because of the intricacies often associated with PCET in large and complex biological systems, the small protein, azurin, is an excellent model for understanding PCET. The native form of azurin has two tyrosines and a single tryptophan, the latter of which exists as a long-lived neutral radical when photolyzed in the presence an exogenous electron scavenger (see Ch.4). Spectroscopic characteristics of the native neutral tryptophan radical have opened doors for the analysis of possible PCET pathways in the protein.[21]

We showed that considerably high pK_a values exist for both of the native tyrosines due to the hydrophobic environments surrounding each of the phenols (see Chapter 3). Because of the presence of nearby hydrogen-bond acceptors as well as small

fraction of solvent exposure, there is motivation to determine whether or not there is quenching of the tryptophan neutral radical via tyrosine oxidation.

The generation of the neutral tryptophan radical via a solvated electron pathway has been studied using a tyrosine-free mutant in the presence of various electron scavengers, and was described extensively in the previous chapter. Using $[Co^{III}(NH_3)_5Cl]Cl_2$ as an exogenous electron quencher, a maximum quantum yield was obtained, providing an experimental method for comparing quantum yields in the presence of the native tyrosines. This chapter describes these experiments to probe the role of tyrosine in azurin redox chemistry.

5.2 Materials and methods

5.2.1 Preparation of single-tyrosine mutants and nitrotyrosine mutants

Azurin mutants were prepared via single-site mutagenesis. For nitrotyrosine samples, nitration procedures were adapted from Dr. Crystal Shih and Dr. Brian Leigh[32] using purified protein and 2% tetranitromethane. Under nitrogen gas, 50 – 100 μM of WT azurin and single-tyrosine mutants were nitrated at pH 12 as described in section 2.1.9.

5.2.2 Preparation of samples for photolysis and photolysis set-up

Samples were prepared in phosphate buffer pH 7.2 and deoxygenated in a 2 mm by 10 mm atmospheric cuvette as discussed in section 2.2.2. An excitation source of 290 nm light was obtained by directing white light from a xenon arc lamp (LuxteL LLC, Danvers, MA) into a monochromator. The sample was photolyzed along the 2 mm pathlength of the cuvette, where the sample was stirred via stir plate apparatus and manual gentle shaking every 30 seconds.

5.2.3 Calculation of W48• quantum yields

W48• quantum yields were determined by dividing the number of neutral tryptophan molecules by the number of excited tryptophan molecules as discussed in section 2.3.3.

5.3 Results

5.3.1 Photolysis of single-tyrosine mutants

Maximum quantum yields of W48• were achieved with $[Co^{III}(NH_3)_5Cl]Cl_2$ exogenous quencher, so photolysis was performed on zinc-substituted species of WTAz (ZnWT) and single-tyrosine mutants (ZnY72 and ZnY108) in the presence of this quencher. The difference absorption spectra of ZnWT, ZnY72, and ZnY108 after 15 minutes of photolysis at pH 7.2 were similar in spectral profile to the difference absorption spectrum of ZnW48. Quantum yields for the W48• radical were determined based on the absorbance at 515 nm and calculated as discussed in Section 2.3.3. A comparison of these yields are recorded in Table 5.1.

Table 5.1: Summary of W48• quantum yields for azurin mutants. The protein:quencher ratio was 1:1 in all samples.

Az Sample	Quencher	pH	$\Phi_{W48\bullet/W48*}$
ZnW48	$[Co^{III}(NH_3)_5Cl]^{2+}$	7.2	0.080±0.010
ZnWT	$[Co^{III}(NH_3)_5Cl]^{2+}$	7.2	0.042±0.013
ZnWT	$[Co^{III}(NH_3)_5Cl]^{2+}$	4.5	0.055±0.003
ZnWT	$[Co^{III}(NH_3)_5Cl]^{2+}$	9.0	0.040±0.004
ZnY72	$[Co^{III}(NH_3)_5Cl]^{2+}$	7.2	0.063±0.009
ZnY108	$[Co^{III}(NH_3)_5Cl]^{2+}$	7.2	0.055±0.013
ZnF110Y	$[Co^{III}(NH_3)_5Cl]^{2+}$	7.2	0[a]
ZnY72NO_2	$[Co^{III}(NH_3)_5Cl]^{2+}$	7.2	0.019[a]

[a]Photolysis experiments for these mixtures were performed only once.

5.3.2 Photolysis of ZnF110Y

Previously, a cation-π interaction between W48 and F110 in azurin was proposed as a possible deprotonation pathway for the generation of the kinetically stable W48•.[21] To probe this pathway, F110 was mutated to tyrosine in an attempt to destabilize the cation-π-like interaction that allows for deprotonation of $W48^{\bullet+}$. This zinc-substituted mutant, ZnF110Y, was photolyzed in the presence of $[Co^{III}(NH_3)_5Cl]^{2+}$ at pH 7.2. Preliminary results indicate a quantum yield of 0 after photolysis of this mutant, suggesting that the proton path was eliminated.

5.3.3 Photolysis of nitrotyrosine azurin

The labeling yield for nitration was greater for the Y72 residue in comparison to the Y108 residue, so photolysis experiments were only performed on the $ZnY72NO_2$ mutant. The difference absorption spectrum of this mutant after 15 minutes of 290 nm photolysis with $[Co^{III}(NH_3)_5Cl]^{2+}$ is presented in Fig. 5.1 and is compared to the difference absorption spectrum of ZnY72 with $[Co^{III}(NH_3)_5Cl]^{2+}$. Quantum yield calculations were determined using extinction coefficients at 280 nm for both ZnY72 and $ZnY72NO_2$ ($\epsilon_{280nm}^{ZnW48-Y72} = 6490\ M^{-1}cm^{-1}$, $\epsilon_{280nm}^{ZnW48-Y72NO_2} = 9350\ M^{-1}cm^{-1}$).[25, 33] The sample consisted of 87% $ZnY72NO_2$, the rest of which was un-nitrated ZnY72. After taking into account this labeling yield, a quantum yield of 0.019 was calculated for $ZnY72NO_2$, which is a 70% decrease in quantum yield from that of the mutant ZnY72 and a 76% decrease from that of the quantum yield for ZnW48.

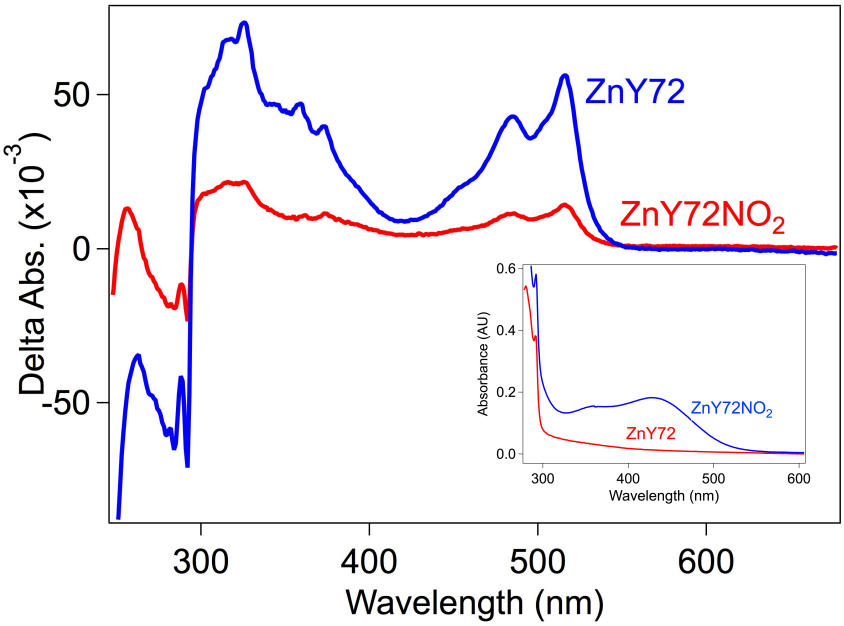

Figure 5.1: Difference absorption spectra of 70 μM ZnY72 and 70 μM $ZnY72NO_2$ photolyzed for 15 minutes in the presence of $[Co^{III}(NH_3)_5Cl]^{2+}$ in 20 mM phosphate buffer, pH 7.2. *Inset*: Steady-state absorption spectra of the samples ZnY72 and $ZY72NO_2$ with $[Co^{III}(NH_3)_5Cl]^{2+}$ prior to photolysis.

5.4 Discussion

Long-range electron transfer reactions in biological systems often rely on amino acid radical intermediates. Often these processes are dictated by a residue's optimized position and the presence of nearby charged residues that influence thermodynamic and kinetic parameters. In azurin specifically, a long-lived neutral tryptophan radical is generated via photoejection of an electron in the presence of an exogenous electron quencher. We report on the quenching of this tryptophan radical via proton-coupled electron transfer from one of two native tyrosine residues and the specific role of local hydrogen-bonding environment in facilitating charge transfer over long distances.

Quenching of the tryptophan cation radical in azurin via charge transfer sheds light on possible PCET reactions via native tyrosine radicals. Photoexcitation of the native tryptophan in zinc azurin in the presence of an exogenous quencher results in photoejection of an electron followed by deprotonation of the cation radical to form a long-lived, stable neutral radical. The yield of radical formation per photoexcited tryptophan was maximized when the tyrosine-free mutant, ZnW48, was photolyzed in the presence of an irreversible exogenous quencher, $[Co^{III}(NH_3)_5Cl]^{2+}$. In this process, the photoexcited tryptophan is highly reducing and can have multiple pathways depending on protein concentration, pH, and the identity and concentration of the exogenous quencher. Maintaining a protein concentration of ~50 μM removed the possibility of collisional quenching and because quantum yields for the radical increased minimally with increasing quencher concentrations, a 1:1 ratio of protein:quencher could be used as a foundation for studying other radical quenching possibilities. These established standards

were key for analyzing quenching of the cation radical via charge transfer from the native tyrosines in azurin.

Tyrosine radicals and their role in charge transfer events have long been studied in protein systems. Most notably, TyrZ, one of the redox-active tyrosines in photosystem II, exemplifies how the formation of a tyrosine radical intermediate via proton-coupled electron transfer is key for the oxidation of the oxygen-evolving complex.[63, 13] In azurin, the two native tyrosines, Y72 and Y108, are 14.5 Å and 8.8 Å from the W48 residue, respectively, and give evidence for a possible PCET reaction in this small protein. The yield of tryptophan radical formation per photoexcited tryptophan decreases by 35% in the presence of both tyrosines and by 15%-25% in the presence of a single tyrosine. To understand participating residues for ET from each of these tyrosines to tryptophan, we performed ET pathway calculations using Harlem software.[64] If Y72 were the redox-active tyrosine responsible for quenching the neutral radical, the calculations suggest that the electron would tunnel through a carboxylate group on D71 and through the backbone N47 (Fig. 5.2). If Y108 were the redox-active tyrosine, electron tunneling would occur through the backbone of M109. The timescale for tyrosine oxidation is not known, but must be occurring before deprotonation of the tryptophan cation radical .[65, 66] A model for the electron transfer and subsequent deprotonation of tryptophan is outlined in Fig. 5.3.

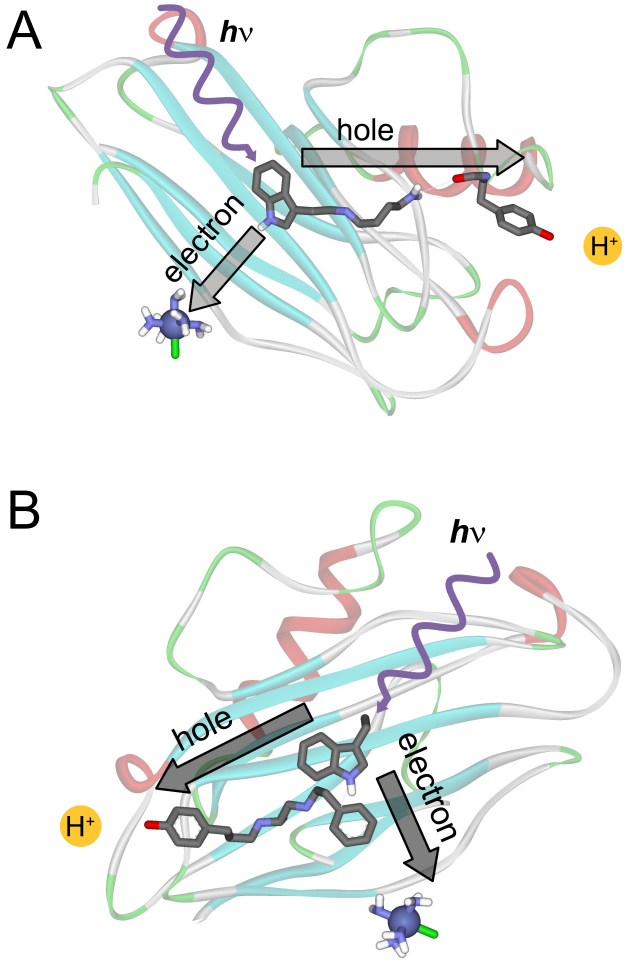

Figure 5.2: Crystal structure of azurin (4AZU) showing residues involved in proposed proton and electron transfer pathways for charge transfer from (A) Y72 and from (B) Y108. Upon photolysis, the ejected electron is scavenged by the indicated exogenous scavenger $[Co^{III}(NH_3)_5Cl]^{2+}$.

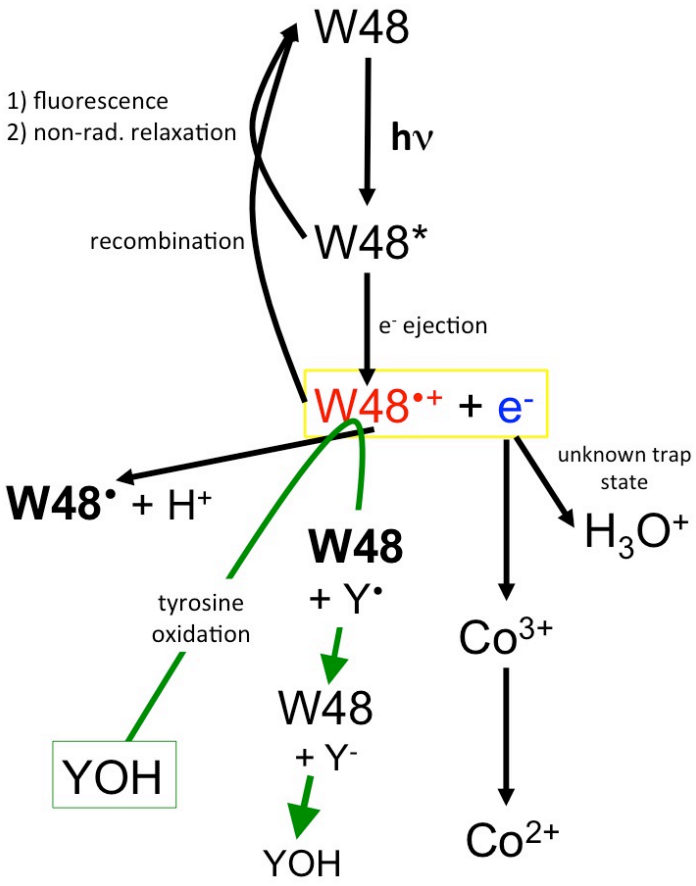

Figure 5.3: Model for the electron transfer and subsequent deprotonation pathways of tryptophan and tyrosine upon photo-excitation of single-tyrosine azurin mutants.

Deprotonation of tyrosine is a necessary component for PCET and is largely influenced by local environment effects. The reported decrease of radical quantum yields in the presence of tyrosine suggests that a certain amount of $W48^{\bullet+}$ is being reduced by either Y108 or Y72, even at the given pH of 7.2 that is below the tyrosine pK_as. As previously discussed (Section 3.3), the protein environments of both Y72 and Y108 likely play a considerable role in these PCET reactions. The hydrophobic environment and presence of a nearby glutamate that may act as a hydrogen bond acceptor with the phenol of the tyrosine help explain the anomalously high pK_a of Y108. A hydrophobic environment also surrounds Y72 but there is greater solvent exposure of the phenol than Y108, and this exposure may facilitate easier deprotonation of this residue. The dependence of quantum yield on pH has been thoroughly studied and has been observed in several proteins such as chymotrypsin.[67] Beyond a certain pH, azurin will likely undergo a strain from electrostatic repulsion, and irradiation may induce denaturation. Preliminary pH dependent photolysis studies of ZnWT + $[Co^{III}(NH_3)_5Cl]^{2+}$ reveal the effect that protonated tyrosine may have on W48•. In comparison to radical quantum yields from the ZnW48 + $[Co^{III}(NH_3)_5Cl]^{2+}$ at pH values of 4.5, 7.2 and 9 (see Table 4.1), all quantum yields from photolysis of ZnWT + $[Co^{III}(NH_3)_5Cl]^{2+}$ at these same pH values are reduced by 0.03 to 0.04 units (Table 5.1). However, because the trend of increasing radical quantum yield with decreasing pH is similar between ZnWT and ZnW48, we cannot verify a conclusion on how the protonation states of these tyrosines mediate radical quantum yields. Nonetheless, the presence of tyrosine in the zinc mutants reduce tryptophan radical quantum yields relative to those obtained from photolysis of ZnW48 and implies the possibility of PCET from tyrosinate to tryptophan.

Quenching of $W48^{\bullet+}$ was also studied through the implementation of unnatural amino acid, nitrotyrosine. Nitrotyrosine has been used to shed light on PCET in other proteins such as in ribonucleotide reductase where the pK_a of a given tyrosine was reported to have decreased by greater than 2.5 units when nitrated.[25, 68] A decrease in both of the tyrosine pK_as in azurin offers further possibility of observing a quenched $W48^{\bullet+}$ radical via quantum yield analysis. A 76% decrease in quantum yield for $ZnY72NO_2$ in comparison to ZnW48 offers preliminary results that would be consistent with past studies of radical quenching via unnatural amino acid PCET in other proteins.[25, 69] Also, because the labeling efficiency was 87%, we take into account the measured quantum yield for Y72 and predict that ~25% of the radical absorbance contribution is attributable to radical formation in un-nitrated ZnY72. Given these results at a pH of 7.2, a pH below the pK_a of 6.71 for $Y72NO_2$ would decrease the quantum yield because of efficient ET from nitrotyrosinate to tryptophan. Ultimately, the observation of a decreased pK_a coupled with a resulting decreased quantum yield supports our hypothesis of tyrosine to tryptophan ET in azurin and provides a framework for studying PCET reactions in other biomolecules.

6 Conclusion and Future Studies

6.1 Summary

Long-range electron transfer is fundamental to all living things – the mechanisms by which nature enhances redox activity in proteins provides life with the sustainable energy that it requires. In order for some catalytic proteins to function as efficiently as they do, they utilize electron hopping across long distances via charge intermediates. For example, the evolution of oxygen in Photosystem (II) and the biosynthesis of DNA by RNR are made possible by specific intramolecular ET paths between donor and acceptor as well as finely-tuned driving forces.[11, 12, 13, 39] Both of these important enzymes take advantage of amino acid radicals as intermediates in multi-step ET. The coupled tunneling reactions across long distances allows for charge propagation at efficient rates.[1] These electron hopping events are often accomplished by tyrosine and tryptophan radicals, where local environment effects are critical for modulating thermodynamic barriers of ET. In fact, potentials and pK_as are largely influenced by electrostatic interactions.

Amino acids such as tyrosine and tryptophan utilize different mechanisms for charge separation. Tyrosine ET is dependent on simultaneous deprotonation due to a relatively high closed-shell pK_a and a very low cation radical pK_a. In contrast, tryptophan undergoes isolated ET and deprotonation events, and the radical exhibits a higher reduction potential than tyrosine.[2] Nonetheless, local environment effects demonstrate that both residues are capable of serving as key participants in accelerating ET at the rates necessary for biochemical reactions.

Previous studies of the native tryptophan in azurin and the photo-induced tryptophan cation radical, $W48^{\bullet+}$, prompted analysis the two native azurin tyrosines, Y72 and Y108, and possible quenching of this highly reducing radical.[20, 21] Spectrophotometric titrations showed anomalously high pK_as that suggested that it would be thermodynamically and kinetically difficult for $W48^{\bullet+}$ to be fully quenched by either tyrosine. Computational studies further suggested that the hydrophobic pockets surrounding both tyrosines contribute to the enhanced pK_a values. Because concerted deprotonation is necessary for tyrosine PCET,[61] steady-state spectrophotometric evidence of quenched $W48^{\bullet+}$ may be enhanced through a decrease in the thermodynamic barrier or modulation of the local hydrogen bonding environments surrounding the tyrosines.

Our studies provided crucial insights on the previously reported neutral tryptophan radical and the mechanisms by which it is formed. Initially, the copper species of the tyrosine-free mutant of azurin showed a rise in radical absorbance with a concomitant decrease in Cu^{II} LMCT absorbance, providing a basis for the hypothesis of direct electron transfer from W48* to Cu^{II}. However, we have discovered through experiments described in this thesis that the presence of impurity, in the form of zinc azurin, is a significant consideration. Photolysis of standard additions of Cu azurin to Zn azurin revealed an increase in radical quantum yield, indicating that rather than intramolecular ET from tryptophan to the copper center within a single protein, a solvated electron may be generated from W48*. The intermolecular electron transfer process was further explored via photolysis of a zinc tyrosine-free mutant (ZnW48) with various electron scavengers including the tyrosine-free mutants of Cu^{I}Az and Cu^{II}Az as well as the known exogenous quenchers, $[Ru^{III}(NH_3)_6]^{2+}$ and $[Co^{III}(NH_3)_5Cl]^{2+}$. Photolysis of

ZnW48 in the presence of the irreversible quencher, $[Co^{III}(NH_3)_5Cl]^{2+}$ resulted in the highest yields of radical formation, on the order of 7.9%, and provided a basis for proposing a realistic mechanism of ET from W48* to the extrinsic quencher, $[Co^{III}(NH_3)_5Cl]^{2+}$. Other extrinsic quenchers were also successful at creating radical. Lower quantum yields were found when using $[Ru^{III}(NH_3)_6]^{2+}$, suggesting that use of a reversible quencher decreased the yield of radical formation. Photolysis experiments on pure Cu^{II}Az or pure ZnAz yielded essentially no radical. The mixture of Cu^{I}Az and Cu^{II}Az also produced no radical, and a minimal amount of 628 nm Cu^{II} absorbance.

A maximum absorbance of W48• allows for a more accurate upper limit on the extinction coefficient of the radical. Provided that other energetic processes are taking place (fluorescence, non-radiative relaxation, recombination), a ε_{max} for the radical was determined with more accuracy given the highest quantum yield was achieved with the mixture ZnW48 and $[Co^{III}(NH_3)_5Cl]^{2+}$. By better understanding the intermolecular ET process between zinc azurin and exogenous molecules, we can gain a better understanding of steady-state ET processes via tryptophan radical intermediates.

The presence of two tyrosines in addition to the single tryptophan in the native species of azurin provides an interesting platform for radical quenching studies via PCET. With knowledge that the intermolecular electron transfer event takes place after photo-excitation of W48, zinc single-tyrosine mutants (ZnY72 and ZnY108) were utilized to determine relative quantum yields compared to those of the tyrosine-free zinc mutant. Resulting quantum yields of the ZnWT as well as ZnY72 and ZnY108 were slightly lower than those of ZnW48, indicating that a quenching mechanism was occurring at a rate faster than the reported deprotonation rate of $W48^{\bullet+}$ (5×10^6 s^{-1}).[21] In

order for this quenching to occur, tyrosine must participate in PCET where hydrogen bonding, i.e. facile deprotonation, allows for ultrafast ET to $W48^{\bullet+}$. Both of these tyrosine residues exhibit unusually high pK_as, suggesting that at high pHs, it may be possible to observe greater quenching, or reduced quantum yields for formation of the tryptophan radical, however we have not yet pursued such studies. Nonetheless, decreased radical quantum yields in the presence of one or both tyrosines at pH well below both tyrosine pK_as suggest evidence for tyrosine PCET in native zinc azurin.

Research groups have recently utilized unnatural amino acids in order to modulate pK_as and therefore observe ultrafast ET to other electron acceptors.[25, 68, 69] The incorporation of nitrotyrosine into our PCET studies decreased tyrosine pK_as to a more biologically feasible pH that was also closer to the pH of the photolysis experiments. With these results, photolysis studies of one of the nitrated single-tyrosine mutants of zinc azurin, $Zn72NO_2$, gave additional support for tyrosine PCET by the observation of a 4-fold decrease in radical quantum yield at a pH where ~90% of the nitrotyrosine is expected to be deprotonated. These preliminary results demonstrate the utility of nitrotyrosine as a tool for studying PCET and the ability to enhance our understanding of amino acid radical reactivity in electron hopping mechanisms.

The study of amino acid radicals via steady-state absorption spectroscopy offers key information for understanding ET in biological systems. These studies that are presented offer insight into the importance of multi-step ET and the complexity often associated with these mechanisms within a large hydrogen bond network. By understanding the dependence of the local environment on these amino acid radicals, key

hydrogen bonding interactions as well as incorporation of unnatural amino acids can be applied to larger, natural biological systems.

6.2 Future studies

Current pH studies involving photolysis of the zinc tyrosine-free mutant gives insight on H^+ as an exogenous quencher, but of equal importance is the pH dependence of nitrotyrosine for W48• quenching. Because the pK_a values of both nitrotyrosines ($Y72NO_2$ and $Y108NO_2$) are significantly lower than those of the natural tyrosines, pH dependent photolysis of $ZnY72NO_2$ and $ZnY108NO_2$ would shed light on the importance of deprotonation for ET to $W48^{\bullet+}$. At a pH higher than 7.2, photolysis of these mutants in the presence of the irreversible quencher, $[Co^{III}(NH_3)_5Cl]^{2+}$, should result in lower quantum yields given enhanced quenching capabilities of the nitrotyrosine. An opposite result is expected for photolysis experiments at lower pH, where protonated nitrotyrosine will be less likely to undergo deprotonation and thus be unable to undergo oxidation.

As discussed in the literature, the generation of the stable radical W48• is formed by electron ejection and deprotonation along a proposed proton transfer pathway.[21] Recent studies involving influence of the cation-π interaction between W48 and 110F have been made difficult by the instability of azurin once 110F is mutated to Y. However, other current work for this pathway has involved site-directed mutagenesis of a local threonine residue (T17), a polar residue that is thought to help facilitate the release of the proton to solvent.[21] By photolyzing zinc mutants of T17A, T17I, and T17V, radical yield information will give insight on whether or not this residue is involved in $W48^{\bullet+}$ deprotonation. Jennifer Pomponio is currently conducting these research efforts as well as future experiments to understand the possible cation-π interaction with 110F.

The results reported in this thesis in addition to the on-going work involving electron and proton transfer in azurin are valuable for the application to biological systems. By studying the electron transfer capabilities of tryptophan and tyrosine radical intermediates and the local environments that modulate their thermodynamic parameters, we can enhance our knowledge of multi-step electron transfer and how to mediate these events in complex biomolecules.

Resources

1. Gray, H. B.; Winkler, J. R., Long-range electron transfer. *P Natl Acad Sci USA* **2005,** *102* (10), 3534-3539.

2. Harriman, A., Further Comments on the Redox Potentials of Tryptophan and Tyrosine. *J Phys Chem-Us* **1987,** *91* (24), 6102-6104.

3. Marcus, R. A., On the Theory of Oxidation-Reduction Reactions Involving Electron Transfer .1. *J Chem Phys* **1956,** *24* (5), 966-978.

4. Marcus, R. A.; Sutin, N., Electron Transfers in Chemistry and Biology. *Biochimica et biophysica acta* **1985,** *811* (3), 265-322.

5. Beratan, D. N.; Onuchic, J. N.; Hopfield, J. J., Electron-Tunneling through Covalent and Noncovalent Pathways in Proteins. *J Chem Phys* **1987,** *86* (8), 4488-4498.

6. Beratan, D. N.; Onuchic, J. N., Electron-Tunneling Pathways in Proteins - Influences on the Transfer Rate. *Photosynth Res* **1989,** *22* (3), 173-186.

7. Hopfield, J. J., Electron-Transfer between Biological Molecules by Thermally Activated Tunneling. *P Natl Acad Sci USA* **1974,** *71* (9), 3640-3644.

8. Onuchic, J. N.; Beratan, D. N., A Predictive Theoretical-Model for Electron-Tunneling Pathways in Proteins. *J Chem Phys* **1990,** *92* (1), 722-733.

9. Giese, B., Long distance charge transport in DNA: The hopping mechanism. *Accounts Chem Res* **2000,** *33* (9), 631-636.

10. Winkler, J. R., Electron tunneling pathways in proteins. *Current opinion in chemical biology* **2000,** *4* (2), 192-198.

11. Faller, P.; Debus, R. J.; Brettel, K.; Sugiura, M.; Rutherford, A. W.; Boussac, A., Rapid formation of the stable tyrosyl radical in photosystem II. *P Natl Acad Sci USA* **2001,** *98* (25), 14368-14373.

12. Eklund, H.; Uhlin, U.; Farnegardh, M.; Logan, D. T.; Nordlund, P., Structure and function of the radical enzyme ribonucleotide reductase. *Prog Biophys Mol Bio* **2001,** *77* (3), 177-268.

13. Berg, J. M.; Tymoczko, J. L.; Stryer, L.; Stryer, L., *Biochemistry*. 6th ed.; W. H. Freeman: New York, 2007.

14. Andersson, J.; Bodevin, S.; Westman, M.; Sahlin, M.; Sjoberg, B. M., Two active site asparagines are essential for the reaction mechanism of the class III anaerobic

ribonucleotide reductase from bacteriophage T4. *Journal of Biological Chemistry* **2001,** *276* (44), 40457-40463.

15. Stubbe, J.; Nocera, D. G.; Yee, C. S.; Chang, M. C. Y., Radical initiation in the class I ribonucleotide reductase: Long-range proton-coupled electron transfer? *Chem Rev* **2003,** *103* (6), 2167-2201.

16. Cukier, R. I., Mechanism for Proton-Coupled Electron-Transfer Reactions. *J Phys Chem-Us* **1994,** *98* (9), 2377-2381.

17. Reece, S. Y., Nocera, Daniel G., Proton-Coupled Electron Transfer in Biology: Results from Synergistic Studies in Natural and Model Systems. *Annu. Rev. Biochem.* **2009,** *78*, 673-699.

18. Sjodin, M.; Styring, S.; Akermark, B.; Sun, L. C.; Hammarstrom, L., Proton-coupled electron transfer from tyrosine in a tyrosine-ruthenium-tris-bipyridine complex: Comparison with Tyrosine(z) oxidation in photosystem II. *Journal of the American Chemical Society* **2000,** *122* (16), 3932-3936.

19. Miller, J. E.; Bercaw, J. E.; Gray, H. B.; California Institute of Technology. Division of Chemistry and Chemical Engineering. Radical formation and electron transfer in biological molecules. http://resolver.caltech.edu/CaltechETD:etd-05292003-131114.

20. Shafaat, H. S.; Leigh, B. S.; Tauber, M. J.; Kim, J. E., Resonance Raman characterization of a stable tryptophan radical in an azurin mutant. *The journal of physical chemistry. B* **2009,** *113* (1), 382-8.

21. Shafaat, H. S.; Leigh, B. S.; Tauber, M. J.; Kim, J. E., Spectroscopic comparison of photogenerated tryptophan radicals in azurin: effects of local environment and structure. *Journal of the American Chemical Society* **2010,** *132* (26), 9030-9.

22. Nar, H.; Messerschmidt, A.; Huber, R.; Vandekamp, M.; Canters, G. W., Crystal-Structure Analysis of Oxidized Pseudomonas-Aeruginosa Azurin at Ph 5.5 and Ph 9.0 - a Ph-Induced Conformational Transition Involves a Peptide-Bond Flip. *Journal of molecular biology* **1991,** *221* (3), 765-772.

23. Seyedsayamdost, M. R.; Reece, S. Y.; Nocera, D. G.; Stubbe, J., Mono-, di-, tri-, and tetra-substituted fluorotyrosines: New probes for enzymes that use tyrosyl radicals in catalysis. *Journal of the American Chemical Society* **2006,** *128* (5), 1569-1579.

24. Seyedsayamdost, M. R.; Yee, C. S.; Stubbe, J., Use of 2,3,5-F3Y-beta 2 and 3-NH2Y-alpha 2 To Study Proton-Coupled Electron Transfer in Escherichia coli Ribonucleotide Reductase. *Biochemistry* **2011,** *50* (8), 1403-1411.

25. Yokoyama, K.; Uhlin, U.; Stubbe, J., Site-specific incorporation of 3-nitrotyrosine as a probe of pKa perturbation of redox-active tyrosines in ribonucleotide reductase. *Journal of the American Chemical Society* **2010,** *132* (24), 8385-97.

26. Leigh, B. S.; Richards, J.; Gray, H. B.; California Institute of Technology. Division of Chemistry and Chemical Engineering., *Electron transfer through organic and biological molecules*. California Institute of Technology: Pasadena, Calif., 2009; p xiv, 123 leaves.

27. Pace, C. N.; Vajdos, F.; Fee, L.; Grimsley, G.; Gray, T., How to measure and predict the molar absorption coefficient of a protein. *Protein science : a publication of the Protein Society* **1995,** *4* (11), 2411-23.

28. Goldberg, M. a. P., I., *Biochemistry* **1976,** *15* (19).

29. Fasman, G. D., *Handbook of Biochemistry and Molecular Biology*. CRC Press: Cleveland, Ohio, 1976; Vol. 1, p 183-203.

30. Leckner, J.; Bonander, N.; Wittung-Stafshede, P.; Malmstrom, B. G.; Karlsson, B. G., The effect of the metal ion on the folding energetics of azurin: a comparison of the native, zinc and apoprotein. *Biochimica et biophysica acta* **1997,** *1342* (1), 19-27.

31. Lancaster, K. M.; Farver, O.; Wherland, S.; Crane, E. J., 3rd; Richards, J. H.; Pecht, I.; Gray, H. B., Electron transfer reactivity of type zero Pseudomonas aeruginosa azurin. *Journal of the American Chemical Society* **2011,** *133* (13), 4865-73.

32. Shih, C.; Lewis, N. S.; Gray, H. B.; California Institute of Technology. Division of Chemistry and Chemical Engineering., *Electron tunneling and hopping through proteins*. California Institute of Technology: Pasadena, Calif., 2008; p xvii, 127 leaves.

33. Crow, J. P. a. B., J.S., *A Comparison to Methods in Enzymology* **1995,** *7*, 116-120.

34. Montalti, M. C., A; Prodi, L.; Gandolfi, M. Teresa *Handbook of Photochemistry*. 3rd ed.; Taylor and Francis Group lLC: 2006.

35. Kuhn, H. J. B., S. E. ; Schmidt, R. , Chemical Actinometry. *Pure Appl. Chem* **2004,** *76* (12), 2105-2146.

36. Bunce, N. J., *Handbook of Organic Photochemistry*. CRC Press, Inc.: 1989; Vol. 1.

37. Lukacs, A.; Eker, A. P.; Byrdin, M.; Brettel, K.; Vos, M. H., Electron hopping through the 15 A triple tryptophan molecular wire in DNA photolyase occurs within 30 ps. *Journal of the American Chemical Society* **2008,** *130* (44), 14394-5.

38. Page, C. C.; Moser, C. C.; Chen, X.; Dutton, P. L., Natural engineering principles of electron tunnelling in biological oxidation-reduction. *Nature* **1999,** *402* (6757), 47-52.

39. Rappaport, F.; Lavergne, J., Coupling of electron and proton transfer in the photosynthetic water oxidase. *Biochimica et biophysica acta* **2001,** *1503* (1-2), 246-59.

40. Rhile, I. J. M., T. F.; Nagao, H.; DiPasquale, A. G.; Lam, O. P.;; Lockwood, M. A. R., K.; Mayer, J. M., *J. Am. Chem. Soc.* **2006,** *128*, 6075.

41. Hammes-Schiffer, S. a. S., A. V. , *J. Phys. Chem. B* **2008,** *112*, 14108–14123.

42. Cukier, R. I.; Nocera, D. G., Proton-coupled electron transfer. *Annual review of physical chemistry* **1998,** *49*, 337-69.

43. Crow, J. P., Measurement and significance of free and protein-bound 3-nitrotyrosine, 3-chlorotyrosine, and free 3-nitro-4-hydroxyphenylacetic acid in biologic samples: a high-performance liquid chromatography method using electrochemical detection. *Methods in enzymology* **1999,** *301*, 151-60.

44. Minnihan, E. C.; Seyedsayamdost, M. R.; Stubbe, J., Use of 3-aminotyrosine to examine the pathway dependence of radical propagation in Escherichia coli ribonucleotide reductase. *Biochemistry* **2009,** *48* (51), 12125-32.

45. Minnihan, E. C.; Young, D. D.; Schultz, P. G.; Stubbe, J., Incorporation of fluorotyrosines into ribonucleotide reductase using an evolved, polyspecific aminoacyl-tRNA synthetase. *Journal of the American Chemical Society* **2011,** *133* (40), 15942-5.

46. Crow, J. P.; Beckman, J. S., The importance of superoxide in nitric oxide-dependent toxicity: evidence for peroxynitrite-mediated injury. *Advances in experimental medicine and biology* **1996,** *387*, 147-61.

47. Mongan J, C. D., McCammon JA., *J. Comp. Chem. 25*, 2038-2048.

48. Tawfik, D. S., *Nitration of Tyrosines*. Humana Press: 2002.

49. Johannissen, L. O.; Irebo, T.; Sjodin, M.; Johansson, O.; Hammarstrom, L., The Kinetic Effect of Internal Hydrogen Bonds on Proton-Coupled Electron Transfer from Phenols: A Theoretical Analysis with Modeling of Experimental Data. *Journal of Physical Chemistry B* **2009,** *113* (50), 16214-16225.

50. Ugurbil, K., Norton, R.S., Allerhand, A., and Bersohn, R.), Tyrosine emission in the tryptophanless azurin from Pseudomonas fluorescens. *Biochemistry* **1977b,** *16*, 886-894.

51. Kamil Ugurbil, R. B., Tyrosine emission in the tryptophanless azurin from Pseudomonas fluorescens. *Biochemistry* **1977,** *16* (5), 895–901.

52. Narvaez, A. J.; Kalman, L.; LoBrutto, R.; Allen, J. P.; Williams, J. C., Influence of the protein environment on the properties of a tyrosyl radical in reaction centers from Rhodobacter sphaeroides. *Biochemistry* **2002,** *41* (51), 15253-8.

53. Kaila, V. R. I.; Verkhovsky, M. I.; Wikstrom, M., Proton-Coupled Electron Transfer in Cytochrome Oxidase. *Chem Rev* **2010,** *110* (12), 7062-7081.

54. Sato, S.; Yugeta, R.; Shinsaka, K.; Terao, T., Nitrous Oxide as an Electron Scavenger in Radiolysis of Hydrocarbons. *B Chem Soc Jpn* **1966,** *39* (1), 156-&.

55. Head, D.; Walker, D. C., Nitrous Oxide as a Scavenger in Radiolysis of Water. *Nature* **1965,** *207* (4996), 517-&.

56. Bard, A. J. F., L. R., Electrochemical Methods: Fundamentals and Applications. **2001,** *2nd ed*.

57. Gafney, H. D.; Adamson, A. W., Excited-State Ru(Bipyr)32+ as an Electron-Transfer Reductant. *Journal of the American Chemical Society* **1972,** *94* (23), 8238-&.

58. Barrett, J., *Inorganic chemistry in aqueous solution*. Royal Society of Chemistry: Cambridge, 2003; p vii, 184 p.

59. Faller, P.; Goussias, C.; Rutherford, A. W.; Un, S., Resolving intermediates in biological proton-coupled electron transfer: a tyrosyl radical prior to proton movement. *Proc Natl Acad Sci U S A* **2003,** *100* (15), 8732-5.

60. Kamiya, N.; Shen, J. R., Crystal structure of oxygen-evolving photosystem II from Thermosynechococcus vulcanus at 3.7-A resolution. *Proc Natl Acad Sci U S A* **2003,** *100* (1), 98-103.

61. Reece, S. Y. S., J.; Nocera, D. G., *BBA -- Bioenergetics* **2005,** *1706* (232).

62. Irebo, T. J., O,; Hammarstrom, L., *J. AM. CHEM. SOC.* **2008` ,** *130* (9194).

63. Keough, J. M.; Jenson, D. L.; Zuniga, A. N.; Barry, B. A., Proton Coupled Electron Transfer and Redox-Active Tyrosine Z in the Photosynthetic Oxygen-Evolving Complex. *Journal of the American Chemical Society* **2011,** *133* (29), 11084-11087.

64. Hamiltonians to Research Large Molecules. http://www.kurnikov.org/harlem_manual/html/index.html.

65. Moser, C. C.; Keske, J. M.; Warncke, K.; Farid, R. S.; Dutton, P. L., Nature of biological electron transfer. *Nature* **1992,** *355* (6363), 796-802.

66. Szabo, A. G.; Stepanik, T. M.; Wayner, D. M.; Young, N. M., Conformational heterogeneity of the copper binding site in azurin. A time-resolved fluorescence study. *Biophysical journal* **1983,** *41* (3), 233-44.

67. Finkelstein, P.; Mclaren, A. D., Photochemistry of Proteins .6. Ph Dependence of Quantum Yield and Ultraviolet Absorption Spectrum of Chymotrypsin. *J Polym Sci* **1949,** *4* (5), 573-582.

68. Seyedsayamdost, M. R.; Yee, C. S.; Stubbe, J., Use of 2,3,5-F(3)Y-beta2 and 3-NH(2)Y-alpha2 to study proton-coupled electron transfer in Escherichia coli ribonucleotide reductase. *Biochemistry* **2011,** *50* (8), 1403-11.

69. Yokoyama, K.; Uhlin, U.; Stubbe, J., A hot oxidant, 3-NO2Y122 radical, unmasks conformational gating in ribonucleotide reductase. *Journal of the American Chemical Society* **2010,** *132* (43), 15368-79.